

UCSF

UC San Francisco Electronic Theses and Dissertations

Title

Targeted overexpression of 29kD or 70kD fibronectin fragment in bone in transgenic mice

Permalink

<https://escholarship.org/uc/item/3jc8k085>

Author

Han, Qin

Publication Date

2005

Peer reviewed|Thesis/dissertation

Targeted Overexpression of 29kD or 70kD Fibronectin
Fragment in Bone in Transgenic Mice: Increased Bone
Mass and Density and Decreased Mechanical Properties

by
Qin Han

DISSERTATION

Submitted in partial satisfaction of the requirements for the degree of

DOCTOR OF PHILOSOPHY

in

Oral and Craniofacial Sciences

in the

GRADUATE DIVISION

of the

UNIVERSITY OF CALIFORNIA, SAN FRANCISCO

July 1, 2006
Date

Ken W. ...
University Librarian

Degree Conferred:.....

DEDICATION

To the Lord Almighty

To my grandparent

Lanying Chen

To my parents

Weichun Pan and Yueqiu Han

To my family

Valerie Hu and Ganyue Hu

ACKNOWLEDGEMENT

The process of developing oneself into a scholar is a rocky journey and while I struggled to overcome the academic and personal hurdles, I could not have done it without the love and support of great people who guided and accompanied me along this path.

Dissertation Research Committee

Caroline Damsky, Ph.D. Chair

Rik Derynck, Ph.D.

Ruth Globus, Ph.D.

Zena Werb, Ph.D.

Collaborators

Ellen Filvaroff, Ph.D.

Marjolein Van Der Meulen, Ph.D.

Mehdi Balooch, Ph.D.

Ruth Globus, Ph.D.

Thomas Wronski, Ph.D.

Present Damsky Lab Members

Dusko Ilic

Nick Larocque

Terri Sonoda

Past Damsky Lab Members

Barry Sudbeck

Eduardo Almeida

Jae-Beom Kim

Kyle Howerton

Suzaynn Schick

Technical Assistance

Linda Prentice

Urszula Iwaniec

Friends

Hua Zhou

Piam Vacharotayangul

Suzyann Schick

Yichun Zhang

Ying Zhu and Xin Guo

Zheyang Li, Yongmei Hu, Xiaowu Li

ABSTRACT

Targeted Over-expression of 29kD or 70kD Fibronectin Fragment in Bone in Transgenic Mice: Increased Bone Mass and Density and Decreased Mechanical Properties

QIN HAN

Skeletal homeostasis and bone mass are maintained by a delicate balance between osteoblastic bone formation and osteoclastic bone resorption. Whole bone mechanical strength and bone quality are dependent upon both geometric and material properties. Animal models in which specific ECM or ECM integrin receptors are altered or deleted in the whole animal, or specifically in bone, have provided powerful insight into the crucial function of ECM in regulating its own composition, organization and stability, and in addition, bone mass and quality. Ample evidence has suggested that FN regulates ECM organization and osteoblast differentiation and survival *in vitro*. However, the study of fibronectin (FN) function in bone *in vivo* has been hindered by the early embryonic lethal phenotype of FN null mice prior to bone formation

The 29kD and 70kD fragments of the N-terminal matrix assembly domain of FN have been shown to act as dominant-negative inhibitors of FN fibrillar matrix formation *in vitro*. FN fragments can also have cryptic functions not shared by native FN. Therefore, we generated transgenic mice with osteoblast specific over-expression of either the 29kD or the 70kD FN fragment, driven by the osteocalcin promoter.

The primary phenotype of transgenic mice is an increase in cortical bone mass accompanied by an increase in cortical immature woven bone at both D35 and D90 and a decrease in marrow volume at D90 only. The D90 phenotype is attributable at least partially to the increased endocortical bone formation. Besides accelerated new bone matrix deposition, delayed or defective remodeling of woven into lamellar bone matrix may also contribute to the increased woven bone phenotype in transgenic mice. These structural changes also resulted in altered biomechanical properties. Transgenic cortical bone tissue elastic modulus and hardness are significantly lower suggesting weaker material properties, which is consistent with the reduced bone tissue modulus and ductility calculated from a whole-bone strength testing. However, the whole bone strength is not compromised due to the compensation by an increase in bone geometry. Taken together, our results demonstrate that bone-specific over-expression of 29kD or 70kD FN fragment leads to changes in ECM organization, bone mass and bone quality.

Thesis Committee Chairman



Caroline H. Damsky, Ph.D.

TABLE OF CONTENTS

INTRODUCTION	1
Skeletal homeostasis, bone mass and bone mechanical properties	1
ECM and bone mass and quality	3
FN, tissue homeostasis and bone	6
FN fragments	7
Project overview	10
MATERIALS AND METHODS	12
RESULTS	29
Generation of 29kD and 70kD FN transgene expression vectors and their characterization in ROS 17/2.8 osteosarcoma cells (ROS).	29
Generation of 29kD and 70kD FN transgenic mice and characterization of transgene expression and localization in the bone.	40
Phenotypic characterization of 29kD and 70kD FN transgenic mice	47
A dramatic bone phenotype in 29kD FN transgenic line 08 (TG08) is unlikely relevant to transgene expression	107
DISCUSSION	113
FN fragments regulate bone remodeling and/or bone matrix organization	114
FN fragments regulate cortical bone mass	118
FN fragments regulate biomechanical properties of the bone	121
Future directions	126
REFERENCES	129

LIST OF FIGURES

Figure 1	34
Figure 2	35
Figure 3	36
Figure 4	38
Figure 5	39
Figure 6	42
Figure 7	43
Figure 8	44
Figure 9	46
Figure 10	53
Figure 11	60
Figure 12	61
Figure 13	63
Figure 14	70
Figure 15	89
Figure 16	93
Figure 17	102
Figure 18	104
Figure 19	109
Figure 20	110
Figure 21	112

LIST OF TABLES

Table 1	49
Table 2	56
Table 3	68
Table 4	71
Table 5	79
Table 6	81
Table 7	84
Table 8	91
Table 9	95
Table 10	98

INTRODUCTION

Skeletal homeostasis, bone mass and bone mechanical properties

The skeleton is among the most dynamic organs in the vertebrate body, not only during growth, but also throughout life. The balance between bone formation and bone loss is referred to as skeletal homeostasis, and is accomplished by a dynamic process called bone remodeling. A period of initial rapid bone formation occurs during development and during post-natal growth, either directly following mesenchymal condensation (intramembranous bone formation), or by a replacement of a cartilage model (endochondral bone formation). During this period, bone formation greatly exceeds bone remodeling. A period of balanced bone formation and remodeling then occurs, followed by a period in which the rate of bone loss exceeds formation.

Skeletal homeostasis and bone mass are maintained by a delicate balance between bone resorption by hematopoietically-derived osteoclasts and bone formation by mesenchyme-derived osteoblasts. When bone resorption exceeds bone formation, bone mass is progressively compromised. This occurs in certain bone diseases, such as osteoporosis, Paget's disease, and following degeneration of surrounding articular cartilage or periodontal support structures caused by chronic inflammation associated with rheumatoid arthritis or periodontal disease. Emerging evidence implicates calcium availability, sex steroids, hypothalamic relay and mechanical usage in determining skeletal homeostasis and maintaining steady state bone mass (Shun-ichi Harada and Gideon Rodan 2003). Yet, the mechanisms by which bone formation and bone

resorption are regulated and coupled are not fully understood. Mechanical stress and several soluble factors, such as insulin-like growth factor (IGF) and transforming growth factor (TGF β) have been suggested as such “coupling” factors. How mechanical stress is sensed by bone and how signals are transduced to regulate bone mass is a subject under intensive study. The current hypothesis is that mechanical load-induced deformation of bone and strain on the bone extracellular matrix (ECM) is transformed from mechanical energy, through cell membrane stress-sensitive calcium channels and the integrin family of $\alpha\beta$ heterodimeric transmembrane receptors, to chemical energy, in the form of intracellular mechano-signaling complexes. The intracellular mechano-signaling complexes, in turn, affect gene expression, bone homeostasis and bone mass (Pavalko et al., 2003).

However, skeletal homeostasis and bone mass are not the only factors contributing to a healthy skeleton. The functional integrity of the skeleton and its ability to bear mechanical loads, as assessed by whole bone strength test, is influenced by geometric factors (such as size and shape) as well as the material properties of the bone. Bone material properties are the mechanical properties of the constituent materials (collagen, non-collagenous matrix protein and mineral) independent of geometric form of the bone. The material properties are determined by not only the composition but also the organization of the constituent extracellular matrix (ECM) and mineral. Mutations in one of the major constituent of bone matrix, type I collagen, results in defective matrix and mineral composition and/or organization and poor intrinsic bone material quality as demonstrated in human disease osteogenesis imperfecta (OI) (Boskey et al., 1999).

Because ECM molecules and their integrin receptors play key roles in tissue organization and homeostasis in general (Damsky et al., 1997), animal models in which specific ECM or ECM receptor components are altered or deleted in the bone will provide powerful *in vivo* systems to examine molecular basis of bone homeostasis, intrinsic bone material quality control and bone adaptation in response to mechanical loads.

ECM and bone mass and quality

Cell interactions with ECM and with neighboring cells plays crucial roles in the formation, homeostasis and remodeling of a variety of tissues. The interaction between the ECM and bone cells can be direct; through signals from ECM molecules themselves, and indirect; through environmental factors embedded in the ECM and released by the action of matrix degradation (Damsky et al., 1997). In an *in vivo* model of how osteoblast-ECM interactions affect bone, transgenic mice expressing a dominant-negative truncated integrin $\beta 1$ subunit under the control of osteocalcin promoter show defective bone matrix deposition, enhanced bone remodeling, decreased bone mass, and reduced bone strength (Damsky, 1999, Zimmerman et. al., 2000, Globus et. al., 2004 in press). These results suggest that signals from ECM through integrin receptors affect the acquisition of bone mass and bone strength to meet mechanical demands.

Bone ECM is composed of type I collagen and a host of non-collagenous proteins such as osteonectin, biglycan, osteocalcin, osteopontin and fibronectin. The major structural component of the bone ECM is type I collagen. Mutations of type I collagen genes are the molecular basis of 90% cases of human osteogenesis imperfecta (OI) which is characterized by bone fragility, skeletal deformities, and in severe cases, in utero death

(Cole, 1997; Lund et.al., 1997, Kuivaniemi et.al., 1997; Prockop and Kivirikko, 1995; Prockop et.al., 1994). Ultrastructural and biomechanical studies of bones from several murine models of human OI have underscored the importance of collagen structure and collagen matrix organization in bone mass, strength, and material quality (Chipman et. al., 1993; Saban et. al., 1996; Pereira et. al., 1995; Jepsen et. al., 1997; Camacho et. al., 1996 and 1999; and Kozloff et. al., 2004).

The less abundant, non-collagenous components that are characteristic of mature bone ECM, including osteonectin, biglycan, osteocalcin and osteopontin, also show changes in bone mass when these genes are deleted in the mice. Osteonectin and biglycan deficiency lead to decreased bone phenotype; while osteocalcin deficiency result in increased bone phenotype and osteopontin deficiency in increased bone upon challenge. Osteonectin is also known as SPARC (Secreted Protein Acidic and Rich in Cysteine) or BM-40, Osteonectin expression is reduced in OI. Osteonectin-null mice displayed a phenotype of decrease in osteoblast number and bone formation rate. This low-turnover osteopenia suggest that osteonectin is necessary for the maintenance of bone mass and normal remodeling (Delany et. al., 2000). Biglycan is a member of the family of small leucine-rich proteoglycan expressed in bone and cartilage. Targeted disruption of biglycan results in reduced skeletal growth and progressively decreased bone mass with age (Xu et. al., 1998). Ultrastructural analysis of collagen reveals that biglycan deficiency leads to abnormal collagen fibril morphology (Corsi et. al., 2002). Osteocalcin is the most abundant non-collagenous protein in the bone ECM. When osteocalcin is genetically ablated, mice develop a phenotype marked by higher bone mass and bone formation rate

(Ducy et. al., 1996). Osteopontin is an RGDS-containing ECM protein which is a ligand for the $\alpha v \beta 3$ integrin abundantly expressed on osteoclasts. Interestingly, osteopontin (OPN)-deficient mice bones show normal development morphologically (Rittling et. al., 1998). However, more intensive mechanistic studies have substantiated the role of OPN in bone resorption process by osteoclast by applying environmental insults to the mice. OPN deficient mice are resistant to bone resorptive responses induced by ovariectomy, mechanical unloading and PTH (Yoshitake et. al., 1999, Ishijima et. al., 2001, Ihara et. al., 2001).

Taken together, these mutations and deletions in mice reveal that type I collagen, noncollagenous matrix proteins and their organization into a complex bone ECM are functionally important in the regulation of bone homeostasis, bone mass and bone material quality. Fibronectin is also expressed by osteoblasts, especially during early stages of their differentiation. However, deletion of fibronectin (FN) in mice by homologous recombination results in an early embryonic lethal phenotype, prior to bone formation and there are, as yet, no conditional knockouts of the FN function in the skeleton. Therefore, no known animal models address the function of FN in bone *in vivo*.

FN, tissue homeostasis and bone

FN is an extracellular matrix protein initially secreted by cells as a soluble dimer and subsequently assembled into an insoluble fibrillar FN network. Matrix FN can activate integrin signaling to regulate a wide variety of cellular functions such as cytoskeletal

organization, gene expression, matrix remodeling, cell survival and cell growth (Damsky and Werb, 1992; Miyamoto et al., 1996; Giancotti and Rouslahti, 1999; Hocking and Kowalski, 2002; Cukierman et al., 2003). FN also provides a crucial substrate for many forms of cell adhesion and cell migration, such as in embryonic migratory pathways and in the provisional matrix of healing wounds thus playing essential roles in normal development and wound healing (Yost, 1992, Clark, 1996). FN deposition *in vivo* represents the initial event during fibrillogenesis of connective tissue matrices occurring during embryogenesis and wound healing (Colvin, 1989, Thiery, 1989). FN fibrillar matrix also plays pivotal roles in regulating the composition, organization and stability of other ECM proteins, such as type I collagen, type III collagen and thrombosponin-1 (McDonald et al., 1982; Sottile et al., 2002), Tenascin C (Chung and Erickson, 1997), fibulin (Roman and McDonald, 1993; Godyna et al., 1995; Sasaki et al., 1996) and fibrinogen (Pereira et al., 2002).

There is also strong evidence to suggest an important role of FN in bone. *In vivo*, FN is one of the ECM proteins upregulated in pre-cartilage condensations and in the early stages of skeletogenesis (Fischer et al., 1980; Kosher et al., 1989). A role for FN in bone matrix organization is also suggested by its association with individual type I collagen fibrils in the bone matrix, as visualized by ultrastructural immunolocalization studies (Nordahl, 1995). FN expression is highly regulated in bone progenitor cells *in vitro*, with an increase in the early stages of osteoblast differentiation around the same time that type I collagen is upregulated, and a decrease during the late stages of osteoblast maturation (Stein et al., 1990; Winnard et al., 1995; Vary et al., 2000). In addition, FN interactions

with osteoblasts *in vitro* are important for the differentiation of immature calvarial osteoblasts (Moursi, 1996, 1997) and the survival of differentiated calvarial osteoblasts (Globus, 1998). Osteoblast adhesion to FN can transduce signals through RANKL to induce osteoclast maturation *in vitro* (Nakayamada, 2003). FN-induced formation of focal adhesions in osteoblasts *in vitro* have been shown to promote fluid shear stress-induced COX-2 and PGE2 release, both of which are necessary for mechanically induced bone formation. These pieces of evidence suggest that FN may be involved in bone formation and skeletal homeostasis in response to mechanical loads. An animal model of altered FN function *in vivo* in the bone could provide a physiologically relevant system to address this hypothesis.

FN fragments

FN is a heterodimer composed primarily of three types of repeating module (I, II and III) (Hynes, 1990; Pankov and Yamada, 2002). These modules make up protein domains that bind a variety of extracellular and cell surface molecules, including collagen, glycosaminoglycans, fibrin, integrins and FN itself. Fragments containing the assembly domain, such as the 70kD N-terminal fragment can inhibit FN fibrillar network formation (McDonald et al., 1987; McKeown-Longo and Mosher, 1985; Sechler and Schwarzbauer, 1998), and FN lacking this domain is incapable of assembly (Schwarzbauer, 1991; Sottile and Mosher, 1997; Sottile and Hocking, 2002). The 70kD FN contains the amino-terminal 29kD heparin-binding domain and 40 kD collagen binding domain. The active area for formation of FN fibrils lies in the 29kD FN region

(Schwarzbauer, 1991). Thus, both 29kD and 70kD FN block FN fibrillar matrix assembly when added to cultures *in vitro*.

In vivo, FN fragments ranging from 24 to 200 kD are present in elevated concentrations in synovial fluids of patients with rheumatoid arthritis, osteoarthritis and traumatic arthritis (Griffiths et al., 1989; Clemmensen and Andersen 1982; and Xie et al., 1992). FN fragments have also been reported in normal and chronic wound fluid and other pathological body fluids and tissues throughout the body (Carsons, 1987; Easter et al., 1988; Skrha et al., 1988 and 1990; Wysocki and Grinnell 1990; LaCelle et al., 1991; Allal et al., 1992; Suzuki et al., 1992). FN fragments often have cryptic properties not demonstrated by native FN. For example, FN fragments induce MMP activity in number of different cell systems such as synovial fibroblasts (Werb et al, 1989; Huhtala et al., 1995), fibrocartilaginous cells (Hu et al., 2000) and mammary epithelial cells (Schedin et al., 2000). A list of other activities of FN fragments not expressed in native FN is continuously growing: for example, inhibition of proliferation of Schwann cells and endothelial cells (Muir and Manthorpe, 1992; Homandberg et al., 1985); stimulation of expression of tumor necrosis factor in monocyte and mesangial cells (Beezhold and Personius 1992; Lopez-armada et al., 1997) and induction of endothelial-dependent vascular relaxations (Laplante et al., 1988). In-depth mechanistic studies also show that N-terminal 70kD FN co-localizes with matrix FN fibers, stabilizes cell shape and inhibits cell cycle progression and directional migration when added to wounded monolayer endothelial cells in the presence of an established FN-containing matrix (Christopher et al., 1997 and 1999).

Extensive research on the functional consequence of FN fragments, with a focus on 29kD FN, has been carried out in cartilage *in vitro* and *in vivo*. The N-terminal 29kD FN fragment, the N-terminal 50kD collagen-binding FN fragment and other FN fragments induce expression of several matrix metalloproteinases in chondrocytes and cartilage (Bewsey et al., 1996; Stanton et al., 2002; Im et al., 2003; Yasuda et al., 2003; Loeser et al., 2003). They also promote the loss of cartilage proteoglycans (Xie et al., 1994; Homandberg et al., 1997, 1999), chondroadherin (Johnson et al., 2004), collagen type II (Yasuda and Poole, 2002) and the collagen and cell-binding molecules, Cartilage Oligomeric Matrix Protein (COMP). These accumulative catabolic activities result in severe cartilage damage *in vitro* (Homandberg et al., 1992; Xie et al., 1994). 29kD FN fragment can also induce progressive intervertebral disc degeneration when injected into the disc in a rabbit *in vivo* model (Anderson et al., 2003).

FN fragments upregulate many catabolic events observed in cartilage degeneration and osteoarthritis and may also be involved in normal cartilage homeostasis. Thus, we hypothesize that over-expression of the N-terminal 29kD or 70kD FN fragments might affect bone homeostasis and bone quality by acting either as a dominant negative inhibitor of endogenous FN function or by a unique function not shared by native FN. To test this idea, we generated lines of transgenic mice to express 29kD FN and 70kD FN specifically in mature osteoblasts and osteocytes, under the control of osteocalcin promoter.

Project overview

Before we used the 29kD and 70kD transgene constructs for generating transgenic mice, the two constructs were stably transfected into ROS 17/2.8 osteosarcoma (ROS) cells that express constitutively high basal level of osteocalcin, and the expression, secretion, and function of these two transgenes were initially examined *in vitro* in ROS cell culture. The 29kD and 70kD FN fragments are highly expressed and secreted into the culture medium. They are incorporated into the ROS cell ECM and appear to promote its mineralization in culture. However, expression of these two fragments did not seem to interfere with the FN fibrillar matrix formation in ROS cells *in vitro*. This is consistent with the notion that FN fragments could have cryptic functions not shared by native FN. Therefore, we carried on generating and characterizing transgenic mice with bone specific over-expression of 29kD or 70kD FN fragment.

The primary phenotype of transgenic mice is an increase in cortical bone mass accompanied by an increase in cortical immature woven bone at both D35 and D90 and a decrease in marrow volume at D90 only. The D90 phenotype is attributable at least partially to the increased endocortical bone formation. However, the possibility of geometric adaptation in response to poor matrix quality cannot be excluded. Besides accelerated new bone matrix deposition, delayed or defective remodeling of woven into lamellar bone matrix may also contribute to the increased woven bone phenotype in transgenic mice. These structural changes also resulted in altered biomechanical properties of the bone tissue and the whole bone. Transgenic cortical bone tissue elastic modulus and hardness are significantly lower suggesting weaker local material

mechanical properties. This is consistent with the reduced bone tissue modulus and ductility calculated from the whole bone strength test. However, transgenic whole bone strength is not compromised because the weaker material properties are compensated by the increase in bone geometry. Taken together, our results demonstrate that overexpression of 29kD or 70kD FN fragment in the bone affect bone metabolism and result in changes in not only bone mass but also bone quality.

MATERIALS AND METHODS

Expression vector

The expression vectors pOc-29kD FN and pOc-70kD FN for generating transgenic mice were constructed from the backbone plamid SST.MLCH (*Genentech*), which contains a 1.8 kb rat osteocalcin (Oc) promoter fragment (Baker et al., 1992), a 650 bp fragment containing the second intron of the rabbit β -globin gene (O'Hare et al., 1981), and the multiple cloning sites followed by 630 bp of the 3' fragment of the human growth hormone gene that contains the polyadenylation signal. Hemagglutinin (HA)-tag was generated by annealing equimolar oligomers 5'-TCGAGTACCCATACGATGTTCC TGACTATTAGT-3' and 5'-CTAGACTAATAGTCAGGAACATCATGTGGGTAC-3' that leave sticky ends for the restriction enzyme *Xho*I at the 5' and for *Xba*I at the 3' end. These sticky ends enabled cloning of HA-tag into *Xho*I and *Xba*I sites of the SST.MLCH multicloning site. Regions of fibronectin cDNA encoding 29 and 70 kD FN fragments were then inserted between *Afl*III and *Spe*I of the SST.MLCH multicloning site to be in the frame with HA-tag at the 3' end. Identity of gene inserts and vector-insert junctions were confirmed by DNA sequence analysis (*Sequetech*). The expression of the plasmids was verified with analyses of stably transfected ROS 17/2.8 osteosarcoma cells.

Cloning fibronectin cDNA encoding 29 and 70 kD FN fragments

Total RNA was isolated from primary rat fibroblasts using RNeasy Kit (*Qiagen*). FN cDNA encoding 29kD fragment was cloned by Superscript One-Step RT-PCR System (*Gibco*), whereas FN cDNA encoding 70kD fragment was cloned by Superscript First-Strand Synthesis System, followed by PCR using high fidelity Taq polymerase (*Gibco*). The same 5' primer (5'-CTCTCCTCCCATCCACTTAAGATGCTCAGG-3') was used for both fragments. The sequence of the 3' primer for 29 kD FN was: 5'-GTAAGTCTGGGTCACACTAGTCTCCTGGCAGCTGAC-3' and for 70 kD FN fragment was 5'-CTTGAACAGGTCCACTAGTGCCTGGGTAGGTCTG-3'. Primers were designed to generate *A*/III at the 5' and *Spe*I at the 3' end of the cDNA fragment. PCR products were run on 1% agarose gel and purified by Qiex Gel Extraction Kit (*Qiagen*). RT-PCR condition for 29kD FN was: one cycle of 50°C, 30 min., and 94°C, 2 min; and 35 cycles of 94°C 45 s, 55°C 25 s, and 72°C 3 min. RT condition for 70 kD FN is: 42°C for 50 min. PCR condition for 70 kD FN was: one cycle of 94°C, 2 min, and 35 cycles of 94°C 1 min, 55°C 2 min, and 72°C 3 min. Sequences were confirmed by DNA sequence analysis (*Sequetech*) and compared to Genbank gene sequence. No extra ATGs were found upstream of the gene initiation codon.

Cell culture and stable transfection

Osteosarcoma ROS 17/2.8 cells were cultured for 24 h in alpha-MEM medium (*UCSF Cell Culture Facility*) containing 10% fetal bovine serum (FBS). Cells were then co-transfected with pBabe-puromycin and pOc-29kD FN (circular or linearized) or pOc-70kD FN vector (circular or linearized) in the ratio of 1:10 following instructions in

Effectene Transfection Kit (*Qiagen*). Cells were selected with 10 $\mu\text{g/ml}$ puromycin (*Roche*) for seven days. Eight individual clones for each construct were generated by subculturing cells in 96-well plates in one cell per well dilution. Transgene protein expression was evaluated by Western Blotting, protein localization by live cell immunofluorescence, and protein secretion into the culture medium by ^{35}S metabolic labeling and immunoprecipitation in both pools of stably transfected cells and individual clones. For ROS cell differentiation, cells were grown in α -MEM medium containing 10% FBS. After confluence (3 days) the medium was further supplemented with freshly prepared ascorbic acid (100 $\mu\text{g/ml}$) and β -glycerophosphate (5mM) to trigger differentiation. Matrix mineralization was detected by Alizarin Red staining.

Western blotting

ROS stable clones were cultured for 48 h in standard medium [α -Modified Eagle medium (MEM) medium (*UCSF Cell Culture Facility*) containing 10% fetal bovine serum (FBS)]. Cells were then lysed in modified radioimmunoprecipitation assay (RIPA) buffer: 0.15 M NaCl, 10mM phosphate buffer, 1% NP-40, 0.5% sodium deoxycholate, and 0.1% sodium dodecyl sulfate (SDS) containing protease inhibitor cocktail (*Sigma*). Protein concentration was measured using a Bicinchoninic acid (BCA) Protein Assay Kit (*Pierce*), 20 μg of lysates were equilibrated and equal amount of lysates were separated on 12% polyacrlamide gels to detect 29kD FN and on 10% gels to detect 70kD FN. Proteins were transferred onto nitrocellulous membrane (*Schleicher&Schuell*) overnight at 4°C. Membranes were then blocked in 5% milk/TBST containing 0.1 % Tween-20 for 30 min at room temperature and probed for transgene protein expression using the mouse

monoclonal antibody (mAb) against the HA epitope tag at 2 $\mu\text{g/ml}$ (*Covance*). The signal was visualized using HRP-conjugated donkey anti-mouse secondary antibody (*Jackson ImmunoResearch*) and enhanced chemiluminescence (ECL, *Amersham Pharmacia*).

Expression of 29kD FN and 70kD FN protein in bones of transgenic mice was detected in calvaria lysates. Mouse calvariae were freshly dissected free of soft tissues, minced and incubated for 1 h at 4°C in lysis buffer containing 2% sodium deoxycholate, 20 mM Tris-HCl pH 8.8, and protease inhibitor cocktail (*Sigma*). Samples were then centrifuged at 14000 g for 10 min at 4°C. Supernatant (DOC soluble fraction) were kept on ice, whereas DOC insoluble pellets were resuspended in 1% SDS lysis buffer containing 1% SDS, 25mM Tris-HCl pH 8.0, and protease inhibitor cocktail (*Sigma*) and kept on ice for 30 min. Samples were centrifuged again at 14000 g for 10 min at 4°C and SDS soluble supernatant collected (SDS soluble fraction). Protein concentration and transgene expression was determined as described above.

Live-cell immunostaining

To determine localization of exogenously expressed 29kD and 70kD FN in the ROS 17/2.8 cells, ROS stable clones were cultured on glass coverslip for 48 h in standard medium. Cells were rinsed with cold PBS and incubated on ice for 1 h with 10 $\mu\text{g/ml}$ mouse mAb against the HA epitope tag (*Covance*) in PBS. Next, cells were rinsed with ice-cold PBS and fixed with cold 4% paraformaldehyde/PBS on ice for 20 min and then washed three times for 5 min with PBS at room temperature. Cells were then incubated 30 min with 5 $\mu\text{g/ml}$ of biotinylated donkey anti-mouse IgG (*Jackson ImmunoResearch*) in PBS and washed three times for 5 min with PBS. Finally, cells were incubated with

5 μ g/ml FITC-conjugated strepavidin (*Vector*) and to visualize nuclei with 10 μ g/ml Hoechst 33342 (*Molecular Probes*) in PBS for 15 min. Cells were then washed and mounted with Vectashield mounting media (*Vector*).

Metabolic labeling

To determine whether exogenously expressed 29kD and 70kD FN proteins are secreted into culture medium stable transfected ROS cells were cultured in standard medium for 24 h. Cells were then washed twice with methionine-, cysteine-, and L-glutamine-free MEM (*Sigma-Aldrich*). L-[³⁵S]methionine and L-[³⁵S]cysteine labeling mixture (*ARC*) was added at 1.0 mCi/ml in growth medium with methionine and cysteine at 10% of the normal level. Cells were exposed to the labeling medium for 1 h and then to standard medium, which was collected 12 h later. Protease inhibitors (0.5 M PMSF, 1 μ g/ml leupeptin, 2 μ g/ml aprotinin) and 0.1% SDS were added to the medium. 29kD FN or 70kD FN was immunoprecipitated overnight with 1 μ g/ml mouse mAb against the HA epitope tag (*Covance*), whereas FN was immunoprecipitated overnight with 1 μ g/ml anti-FN mAb (*BD Transduction Laboratories*). Precipitates were collected with sheep anti-mouse-conjugated Dynabeads (*Dynal Biotech Inc.*), and separated on 6% SDS-PAGE. Gels were dried and exposed to BioMax MS Imaging Film (*Eastman Kodak*) to detect radiolabeled proteins.

Alizarin red staining

On D21 of ROS cell culture in differentiation medium, the cell layer was washed with phosphate-buffered saline and water, quickly followed by 100% ethanol for fixation. For Alizarin red staining, cell layers were stained with 1% Alizarin red S solution for 30 min and washed with distilled water several times.

Generation of transgenic mice

FVB/N strain (*Taconic*) of 29kD FN or 70kD FN transgenic mice was generated using standard techniques (Hogan et al., 1986). Four μg of each pOc-29kD FN and pOc-70kD FN plasmid were cut with *PvuI*. Linearized 3851 bp fragment containing the 29kD FN and 4841 bp fragment containing the 70kD FN construct were purified using a Qiex Gel Extraction Kit (*Qiagen*). Fragments containing the osteocalcin promoter, 29kD FN or 70kD FN coding sequence, and HA-tag (3851 bp and 4841 bp, respectively) were purified by Qiex Gel Extraction Kit (*Qiagen*) and microinjected into fertilized eggs of FVB/N mice at the UCSF Comprehensive Cancer Center Transgenic Mouse Core Facility. Microinjected eggs were implanted into oviducts of pseudopregnant female mice and carried to term. Positive founders for pOc-29kD FN and pOc-70kD FN were identified by Southern Blot analysis of genomic DNA isolated from mouse tails (Laird et al., 1991). Genotyping of transgenic mice subsequently was carried out by polymerase chain reaction (PCR) analysis of tail genomic DNA with transgene-specific 5' and 3' primers. Founder chimeric male mice were bred to wild-type FVB/N females to generate F1 heterozygotes. These heterozygotes were inbred and phenotype was analysed. All

animals were bred and maintained in UCSF transgenic facility in a controlled environment according to UCSF institutional guidelines.

Southern Blotting

To determine the number of transgene copies integrated in the genome, 10 μ g of genomic DNA isolated from the tails was digested with either *EcoRI*, *EcoRV*, *BamHI*, *HindIII*, or *SacI* overnight at 37°C. Digests were separated on 1% agarose in 1X TBE. The gel was incubated in 0.25M HCL for 30 min in room temperature for depurination and rinsed with ddH₂O three times. The gel then was soaked in 0.5M NaOH/1.5M NaCL for 15 min twice for denaturation and then neutralized twice 15 min each in 0.5M Tris PH7.4/1.5M NaCL. DNA was transferred and crosslinked to Hybond-N Plus nylon membrane (Amersham). The membrane was prehybridized in Quikhyb solution (Stratagene) for 1 h at 68°C and then hybridized at 68°C for 3-4 h with the 800 bp *SmaI-SpeI* fragment of pOC-29kD FN, or with the 860 bp *BsmI-SpeI* fragment of pOC-70kD FN probe labeled with PrimeIt Random Primer Kit (*Stratagene*). Membranes were washed three times for 15 min at 65°C in 2XSSC/1%SDS wash buffer and exposed to Biomax MS film (Kodak) overnight at -70°C.

PCR

Mice were genotyped by PCR using the following primers: 5'-CCAAGGCTGGATGATGGTGGACTGTACTTG-3' (5' primer for 29kD FN mice), 5'-CGACACGTTCCA CAAGCGTCACGAGGAGGGAC-3' (5' primer for 70kD FN mice), and 5'-

GGTCATAGACGTTGCTGTCAGA GGCGATGG-3' (3' primer used for both 29kD FN and 70kD FN mice). PCR condition for genotyping is: 1 cycle of 94°C for 2 min, and 25 cycles of 94°C for 1 min, 60°C 1 min, and 72°C 1 min. The PCR product of 300bp indicated the presence of 29kD FN transgene and the PCR product of 300bp indicated the presence of 70kD FN transgene.

RT-PCR

The presence of 27kD and 70kD FN mRNA in transgenic mice was detected with RT-PCR. Femurs from 35-day-old wild-type and transgenic mice were dissected free of soft tissue, epiphysis, and bone marrow, and then frozen in liquid nitrogen. To isolate total RNA, frozen bones were powdered with mortar and pestle, homogenized with a tissue homogenizer (*Fisher Scientific*) for 30 s in TRIzol reagent (*Gibco*), extracted with chloroform, and precipitated in isopropanol. Total RNA was then treated with DNase I (*Gibco*) for 30 min at 37°C and transgene mRNA expression was detected using Single-Step RT-PCR (*Clontech*). PCR primer sets were the same as primers used in genotyping. RT-PCR conditions were: 1 cycle of 50°C for 30 min and 94°C for 2 min; and 35 cycles of 94°C for 1 min, 60°C for 1 min, and 72°C 1 min.

Immunohistochemistry

Calvariae from 10-day-old mice were dissected, fixed in 4% paraformaldehyde (pfa)/PBS at room temperature for 30 min, decalcified for 3 days at 4°C in 19% EDTA (pH 7.4), then dehydrated in 30% sucrose overnight and embedded in Tissue Tek Optimal Cutting

Temperature compound (OCT) (*Miles*). Saggital 7 μm thick frozen sections were fixed again in 4% pfa/PBS at room temperature for 15 min. Endogenous peroxidase activity was quenched with 0.3% H_2O_2 /methanol for 45 min. Sections were then blocked with Biotin/Avidin Blocking Kit (*Vector*) and 100 $\mu\text{g}/\text{ml}$ ChromPure mouse IgG (*Jackson ImmunoResearch*) in 1% BSA/PBS for 1 h. Exogenously expressed 29kD or 70kD FN fragments were detected with biotinylated mouse mAb against the HA epitope tag (*Covance*) and VECTASTAIN Elite ABC reagents following instructions in the kit (*Vector*). Signal was revealed by incubation in a True Blue peroxidase substrate solution (KPL, Gaithersburg, Maryland) until desired stain intensity was reached and counterstained with Contrast red (KPL, Gaithersburg, Maryland). FN was immunostained using rabbit polyclonal anti-FN Ab (*Sigma*). Signal was visualized using secondary fluorescein-conjugated donkey anti-rabbit Ab (*Jackson ImmunoResearch*).

Gross morphology and radio-opacity of the tibia bones

The structure and the radio-opacity of mineralized bone was determined on tibiae from 35-day and 90-day-old mice dissected free of soft tissues. Length of the bones was determined with electronic calipers. Frontal plane bone microradiographs were taken on Kodak X-OMAT TL film (*Eastman Kodak*) exposed to Faxitron43805N (*Faxitron*) for 1 min at 35kVp. A total of 8 female and 7 male wild type bones; 8 female and 8 male TG#01 bones; 9 female and 8 male TG#10 bones; 6 female and 8 male TG#24 bones; and 9 female and 8 male TG#65 bones were imaged with Faxitron.

Bone mass assay

To determine bone mass, tibiae were dried for 24 h at 100°C in vacuum oven Model 5851 (*National Appliance*), weighed for dry mass, ashed in a muffle furnace (*Sybron/Thermolyne*) at 500°C for 6 h and then weighed again. Ash fraction was defined as bone ash mass/dry mass x 100.

Histological analysis

Tibia from 35-day old and the femur-tibia from 90-day old mice were dissected, fixed in 4% pfa/PBS overnight at 4°C. Tissues were decalcified in 19% EDTA (pH 7.4) at 4°C for 10-14 days, then dehydrated in a graded ethanol series and embedded in paraffin. Hematoxylin and eosin staining was performed on 10 µm-thick adjacent longitudinal sections using standard procedures (Sheehan and Hrapchak, 1980).

Lamellar and non-lamellar bone ratio

The sections were viewed through polarized light to visualize the collagen matrix deposition pattern. The percentage of woven bone is determined as woven bone area/total bone area x 100. Quantification was based on analysis of randomly selected 8 microscopic fields distal to the metaphyseal-diaphyseal junction on each bone section. A total of three longitudinal sections 300 µm apart were quantified for each bone. A total of 6 wild type and 7 transgenic bones from 35-day-old and 5 wild type and 5 transgenic bones from 90-day-old mice were analyzed in this study.

Quantitative micro-computed tomography (μ CT)

Femurs were dissected, fixed in 4% pfa/PBS overnight at 4°C and stored in 70% ethanol on cold until time of testing. Micro-computed tomography (μ CT) was employed to quantify cortical structure of the mouse femur. Femur samples were imaged by a SCANCO Medical (*Basserdorf*) μ CT40 micro-imaging system operating with x-ray tube energy level at 50 keV and a current of 80 μ A. Contiguous axial image slices were obtained with an isotropic voxel size of 16 μ m. System calibration was performed with a hydroxyapatite phantom of known density (2.91 g/cm³). Twenty percent of the full-length of the femur centered at the midpoint of the femoral diaphysis (mid-diaphysis) was selected for analysis. Cortical thickness is deduced from an axial slice through the femur.

The femoral cortical bone and marrow volume were determined by application of an automated image segmentation algorithm constructed from the *Analyze (AnalyzeDirect)* image analysis software libraries that has previously been described (1). The cortical bone volume, marrow volume, total tissue volume, cortical bone density and cortical thickness were determined from the segmented cortical image data.

Histomorphometry

A fluorochrome labeling technique was used to determine active mineralization sites and rates of bone formation. Each mouse was injected subcutaneously with demeclocycline (15mg/kg, Sigma Chemical Co., St. Louis, MO) on the 13th day and with calcein (15 mg/kg; Sigma Chemical Co., St. Louis, MO) on the 7th and 3rd day prior to necropsy.

Quantitative Bone Histomorphometry - Cancellous Bone: After fixation in 4% formalin overnight at 4°C, the 2nd lumbar vertebrae and right distal femora were dehydrated in graded ethanols and xylene and embedded undecalcified in modified methyl methacrylate (1). Frontal sections (4 and 8 μm thick) were cut with a vertical bed microtome (AO Autocut 2165) and affixed to slides precoated with 1% gelatin solution. The 4 μm thick sections were stained according to the Von Kossa method with a tetrachrome counterstain (Polysciences, Warrington, PA), and used for determining bone structural and cellular endpoints. The 8 μm thick sections were left unstained and used for assessing fluorochrome labeling and dynamic measurements of bone formation. Histomorphometric data were collected with the Bioquant Bone Morphometry System (Nashville, TN) and the Osteomeasure (OM) and Trabecular Analysis Systems (TAS) (OsteoMetrics, Inc., Atlanta, GA) and reported in accordance with standard bone histomorphometry nomenclature (2).

For data collection, the sample measurement areas within lumbar vertebral bodies began 0.30 mm from the cranial and caudal growth plates (area mean, 2 mm^2) and included secondary spongiosa only. The sample areas within the distal femoral metaphyses extended between 0.5 and 2.0 mm (area mean, 1.7 mm^2) and between 2.0 and 3.5 mm (area mean, 1.5 mm^2) proximal to the growth plate and also included secondary spongiosa only. Cancellous bone volume was expressed as a percentage of bone tissue area. Microarchitectural endpoints, including trabecular thickness (μm), number (/mm), and separation (μm) were calculated with TAS software from measures of bone perimeter and area (3). The node to terminus ratio (number of trabecular junctions relative to

number of trabecular free ends), an index of trabecular connectivity, was also be measured with the TAS system (4). Osteoclast and osteoblast surfaces were measured in stained lumbar vertebral sections and expressed as percentages of total cancellous bone surface. Fluorochrome-based indices of bone formation, including mineralizing surface (percentage of cancellous bone surface with double calcein label plus single calcein label) and mineral apposition rate, were measured in lumbar vertebral unstained sections. Bone formation rate (total surface referent) was calculated by multiplying mineralizing surface by mineral apposition rate. Cellular and fluorochrome endpoints were not measured in distal femoral metaphyses because of low cancellous bone volume in this area.

Quantitative Bone Histomorphometry - Cortical Bone: After fixation in 4% formalin overnight, the right distal tibiae were dehydrated in graded ethanols (1 change of 70% ethanol, 1 change of 95% ethanol, and 4 changes of 100% ethanol) and defatted in acetone (4 changes of acetone) over a 2-week period. The bone samples were then embedded undecalcified in a polyester resin (Tap Plastics, San Jose, CA) and sectioned cross-sectionally at a thickness of approximately 200 μm between 2 and 3 mm proximal to the tibiofibular junction with an Isomet low speed saw (Buehler, Lake Bluff, IL). The sections were then ground to 20 μm and mounted on a glass slide pre-coated with gelatin for histomorphometric analyses. Cortical bone areas and perimeters and fluorochrome-based indices of bone formation were measured using Osteomeasure (OsteoMetrics, Inc., Atlanta, GA). Specific endpoints included total tissue area (cortical bone + bone marrow), cortical bone area, cortical width, and marrow area. Mineralizing surface (percentage of bone surface with demeclocycline label) and mineral apposition rate

(distance between demeclocycline label and periosteal surface/13 days) were measured at the periosteal surface. Mineralizing surface (percentage of bone surface with both calcein labels) and mineral apposition rate (interlabel distance between the calcein label and 2nd calcein label/4 days) were also measured at the endocortical surface. Endocortical bone formation rate was determined by multiplying mineralizing surface by mineral apposition rate.

Assessment of biomechanical properties (three-point bending test)

The biomechanical properties: the whole bone strength, stiffness, and post-yield deformation were evaluated after normalizing for the specimen geometry on femurs of the 90-day-old mice using a three-point bending protocol. The femurs were harvested with intact surrounding soft tissues immediately after sacrifice, wrapped in saline-soaked gauze, sealed in scintillation vials and stored at -20°C until time of testing.

X-ray images in the anterior-posterior and medial-lateral planes were taken and the two axis dimensions of the femoral diaphysis were measured at both the periosteal and endosteal surfaces. These dimensions were used to calculate the area moment of inertia (I , mm^4). The whole bone was loaded to failure at a displacement rate of 0.05 mm/s. The central load was applied to the anterior surface of the femoral diaphysis with a 7-mm span for all tests. Maximum bending moments (M_m , N-mm), failure bending moments (M_f , N-mm), maximum displacement (D_m , mm), failure displacement (D_f mm) and bending stiffness (EI , $\text{N}\cdot\text{mm}^2$) were calculated from the load-displacement data.

Different maximum and failure deformations indicate post-yield deformation. Bone tissue effective modulus (EI/I , N-mm⁶) was defined as EI normalized by bone geometry-moment of inertia.

Atomic force microscopy (AFM) and nanoindentation

A modified atomic force microscope (AFM; Nanoscope IIIa (*Veeco*) combined with nanoindentation transducer (*Hysitron*) was used to measure elastic modulus (E) and hardness (H) of the bone material. Humerus of one transgenic and one wild type mouse were embedded, without fixation, parallel to each other in one block of methylmetacrylate. Specimens were cut with continuous water irrigation till marrow was exposed and then polished first with successive grades of silicon carbide paper, followed by progressively finer grades of diamond slurry (down to 0.05 μm) until a smooth surface was attained. The AFM nanoindentation was performed on two different locations in the compact bone with four specimens each from the transgenic and wild type mice. All indentations were performed with 700 μN maximum load. Twenty-four indents of each location were made covering a typical 15 μm^2 area. The elastic modulus and hardness were calculated from the unloading force/displacement slope at a maximum load and the projected contact area at this load.

The local mechanical property determination using “discrete indentation” technique had inherent limited lateral resolution ($\sim 2 \mu\text{m}$) to avoid interaction between consecutive indents. Further modification of the instrument allowed “dynamic stiffness” mapping

(DSM) to obtain viscoelastic modulus images applicable to biological materials. In an AFM contact mode, a sharp tip was scanned over a sample with a small sinusoidal modulation force slightly indenting in the elastic zone. The resultant displacement amplitude and its phase with respect to the applied force were recorded and used to calculate the complex elastic modulus with the real component designated as storage, and the imaginary component as loss modulus. For hard tissues such as bone, the storage modulus is essentially equal to the elastic modulus due to a negligible loss modulus value. The technique provides 65836 elastic modulus pixel readings and with a lateral resolution of up to 20 nm in a single image. Bones of total of four wild type and four transgenic mice were analyzed.

Statistical analysis

The mean and standard deviations were reported at each time point for animal weights, **bone** length, biochemical markers of bone remodeling, cortical bone structural **measurements** by μ CT, histomorphometric variables, and mechanical and material **properties** variables. Multiple comparisons of transgenic mice and wild type mice were **analyzed** for significance with one-way ANOVA and with Fisher's protected least **significant** difference posthoc test. Significance was established at $p < 0.05$.

RESULTS

Generation of 29kD and 70kD FN transgene expression vectors and their characterization in ROS 17/2.8 osteosarcoma cells (ROS).

FN is composed of several protein domains which bind a variety of extracellular and cell surface molecules including collagen, glycosaminoglycans, fibrin, integrins and FN itself (Figure 1). FN is secreted by cells as a soluble dimer and is subsequently assembled into an insoluble fibrillar FN matrix. The N-terminal 70kD FN domain contains the N-terminal 29kD matrix assembly domain and the 40kD collagen binding domain. Fragments of FN containing the N-terminal 29kD or 70kD FN domains can inhibit FN fibrillar matrix formation *in vitro* (Schwarzbauer, 1991, Sechler and Schwarzbauer, 1998). FN is easily degraded into fragments and levels of native FN and FN fragments are greatly elevated in a number of pathological body fluids and tissues including synovial fluids and cartilage in rheumatoid arthritis and osteoarthritis, and wound fluid in chronic nonhealing wounds (Griffiths et al., 1989; Xie et al., 1992; Wysocki and Grinnell 1990). In particular, the 29kD FN fragment and the neighboring 50kD FN fragment that contains the collagen-binding domain, but not the native FN, are potent regulators of cartilage metabolism (Homandberg 1999, 2001). In endochondrial bone formation *in vivo*, FN expression is upregulated in hypertrophic cartilage and is highly expressed at the periosteal bone surface and immature bone matrix and then downregulated in mineralized bone matrix with low level of expression in osteocytes (Moursi et al., 1996 and Q. Han, unpublished observations). Elevated FN expression has also been correlated with high

bone turnover triggered by PTH treatment or in bone diseases such as osteogenesis imperfecta (OI) and Paget's disease. It is therefore reasonable to speculate that FN fragments could be generated *in vivo* in the continuing process of bone resorption and bone formation throughout life, and that chronic, excessive release of such fragments could affect bone metabolism. Further support for this hypothesis comes from *in vitro* studies from this laboratory showing that FN plays important roles in osteoblast differentiation and survival in cultured primary calvarial osteoblasts and that introduction into these cultures of FN fragments can disrupt these processes (Moursi et al., 1996, Globus et al., 1998). To test the function of FN and the consequences of chronic expression of N-terminal FN fragments *in vivo* in bones, we designed transgene expression vectors to overexpress N-terminal 29kD or 70kD FN fragments under the control of the bone-specific osteocalcin promoter.

The 29kD and 70kD FN transgene expression vectors for generating transgenic mice were constructed from the backbone plasmid SST.MLCH which contains a 1.8 kb rat osteocalcin (Oc) promoter fragment, a β -globin gene intron and the multiple cloning sites followed by a 3' fragment of the human growth hormone gene that contains the polyadenylation signal (Figure 1). First, rat FN cDNA encoding the N-terminal 29kD FN or 70kD FN fragments was cloned by RT-PCR using primary rat fibroblast. Sequences were confirmed by DNA sequence analysis and compared to Genebank gene sequence. No extra ATGs were found upstream of the gene initiation codon. Second, 29kD FN and 70kD FN were cloned in frame with a C-terminal HA epitope tag into the backbone plasmid. Identity of gene inserts and vector-insert junctions were confirmed by DNA

sequence analysis. The HA epitope tag allowed for specific detection of the 29kD and 70kD FN transgene protein. Further, transgene expression is driven by osteocalcin promoter in the backbone plasmid. Characteristics of this promoter enables transgene expression specifically in mature osteoblasts and osteocytes (Bronckers et al., 1985; Groot et al., 1986; Baker et al., 1992; Mikuni-Takagaki et al., 1995) and the promoter is not highly active until after the initial skeletal patterning (Ducy et al., 1997). Linearized portion of these two circular plasmids containing the osteocalcin promoter, the β -globin gene intron, 29kD FN or 70kD FN coding sequence with the C-terminal HA-tag and polyadenylation signal were generated by PvuI enzymatic digestion and gel purification (Figure 2). Linearized plasmids, not the original circular plasmids were selected for making transgenic mice because of the higher genomic integration rate of linearized DNA in comparison to circular DNA.

Before we used the 29kD and 70kD transgene constructs for generating transgenic mice, the two constructs were stably transfected into ROS 17/2.8 osteosarcoma (ROS) cells and the expression, secretion, and function of these two transgenes were initially examined *in vitro* in ROS cells, which constitutively express high basal level of osteocalcin in culture. ROS cells were stably transfected with either the circular or the linearized form of the 29kD FN or 70kD FN transgene expression vector. Protein expression of the 29kD FN or 70kD FN transgene from both the linear and circular constructs was verified by Western blotting with an HA epitope tag antibody (Figure 3A). Secretion of FN and the 70kDFN transgene in the conditioned medium was demonstrated by immunoprecipitation of ³⁵S metabolically labeled cell culture medium with FN and HA epitope tag antibody

respectively (Figure 3B). Secretion and incorporation of the 29kD FN or 70kD FN into the endogenous FN fibrillar matrix were shown by live cell immunofluorescence with HA antibody alone (Figure 4 top panel) and by live cell co-immunofluorescence with HA and FN antibody (Figure 4 lower panel). To note also from FN staining, these two fragments did not seem to interfere with FN matrix assembly in the early stage of monolayer ROS cell culture. Therefore, we selected high-expressing ROS clones to determine whether there were effects of FN fragment expression on differentiation and matrix mineralization. ROS cells were cultured in differentiation medium (containing ascorbate and β -glycerolphosphate) for 21 days post confluence. Surprisingly, all 3 clones of cells expressing 29kD FN and 4 clones of cells expressing 70kD FN deposited significantly higher amounts of mineralized matrix in comparison to a pool of ROS cells with stable integration of an empty control vector (Figure 5).

Taken together, overexpression of 29kD and 70kD FN transgenes in ROS cells has shown that: 1) 29kD and 70kD FN transgene are expressed at the protein level; 2) Like endogenous FN, these fragments can be secreted by the cells into the cell culture medium or incorporated into the ECM; 3) They appear to promote increased mineralization of the extracellular matrix in these osteosarcoma cells, which ordinarily produce little mineralized matrix *in vitro*. Though this level of transgene expression did not seem to interfere with the FN fibrillar matrix formation in ROS cells *in vitro*, we reason that the cell and matrix environment and remodeling dynamics are very different *in vivo* in bone, and that chronic expression of matrix fragments could have cryptic functions not shared

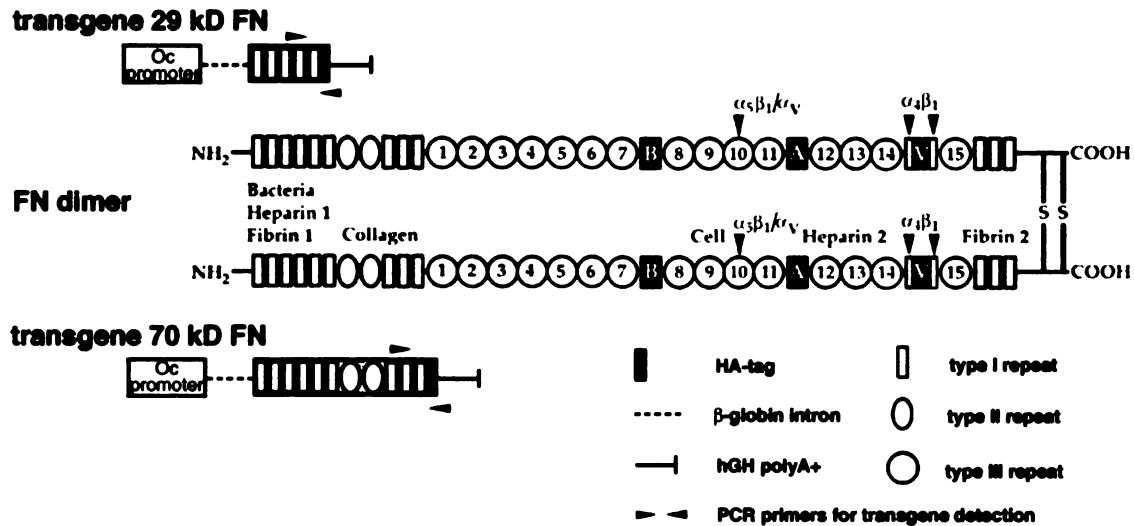


Figure 1. Schematic representation of FN domain structure and 29kD or 70kD FN transgene expression vectors. FN is secreted as a disulfide-bonded dimer composed primarily of three types of repeating module (I, II and III). Sets of modules constitute binding domains for extracellular and cell surface molecules, as indicated. The 29kD N-terminal fragment (29kD FN) contains the N-terminal matrix assembly domain (the first five type I repeats), which is essential for FN fibrillar matrix formation. The 70kD N-terminal fragment (70kD FN) includes the assembly domain and the 40kD collagen-binding domain. Osteocalcin (Oc) promoter is used to target 29kD and 70kD FN transgene expression specifically to mature osteoblasts and osteocytes in bone. HA-epitope tag at the C-terminus of the transgene enables specific detection of the transgene protein expression. The position of the β -globin intron, the hGH polyA⁺ and the primers for PCR analysis, are also indicated.

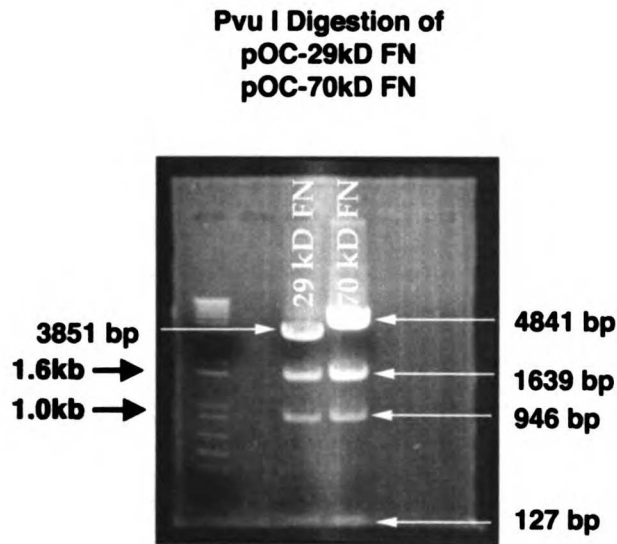


Figure 2. Linearization of 29kD and 70kD FN expression vectors. Circular transgene expression vectors are linearized with PvuI. The 3851 bp and 4841bp bands were purified and used to create 29kD and 70kD FN transgenic mice, respectively. Each linearized fragment consists of the osteocalcin promoter, the β -globin intron, the 29kD FN or 70kD FN coding sequence, with a C-terminal HA tag, followed by a 630bp 3' fragment of the human growth hormone gene that contains the polyadenylation signal. The other three lower bands are fragments created by PvuI cut sites in the vector backbone.

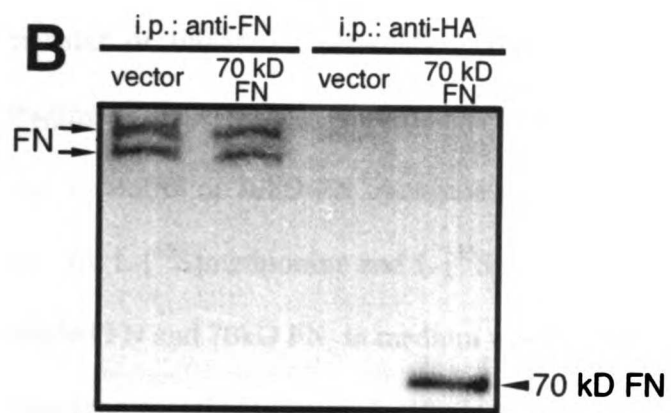
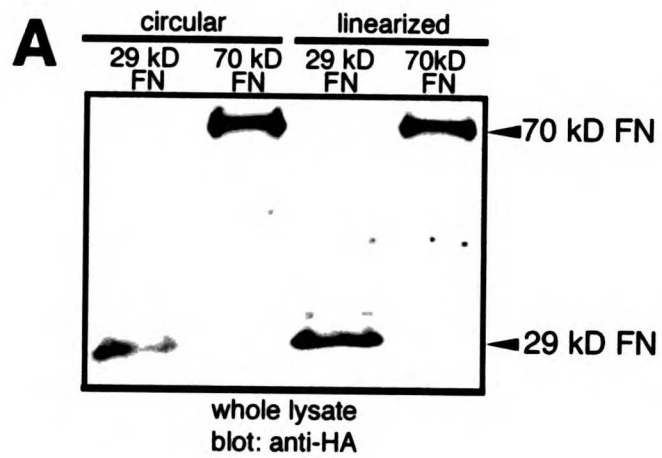


Figure 3. 29kD FN and 70kD FN transgene proteins are expressed and secreted into culture medium in ROS 17/2.8 osteosarcoma cells. (A) Western blot analysis of 29kD and 70kD FN transgene protein expression in ROS cells. ROS cells were stably transfected with circular or linearized 29kD or 70kD FN transgene expression plasmids. Cells were cultured for 48 hours and then lysed. 29kD and 70kD FN transgene protein expression levels were detected with anti-HA epitope tag antibody. The 29kD and 70kD FN bands were detected in lysates of ROS cells with stable integration of either the circular or linearized plasmids. (B) Detection of radiolabeled FN and 70kD FN fragments in ROS cell conditioned medium. ROS cells were stably transfected with vector control or 70kD FN transgene plasmid. Proteins were labeled with a pulse of 1.0 mCi/ml L-[³⁵S]methionine and L-[³⁵S]cysteine mixture for one hour. Distribution of ³⁵S labeled FN and 70kD FN in medium was followed after 12 h. Data suggest that 70kD FN transgene protein is detected only in the conditioned medium of ROS cells with stable integration of 70kD FN transgene.

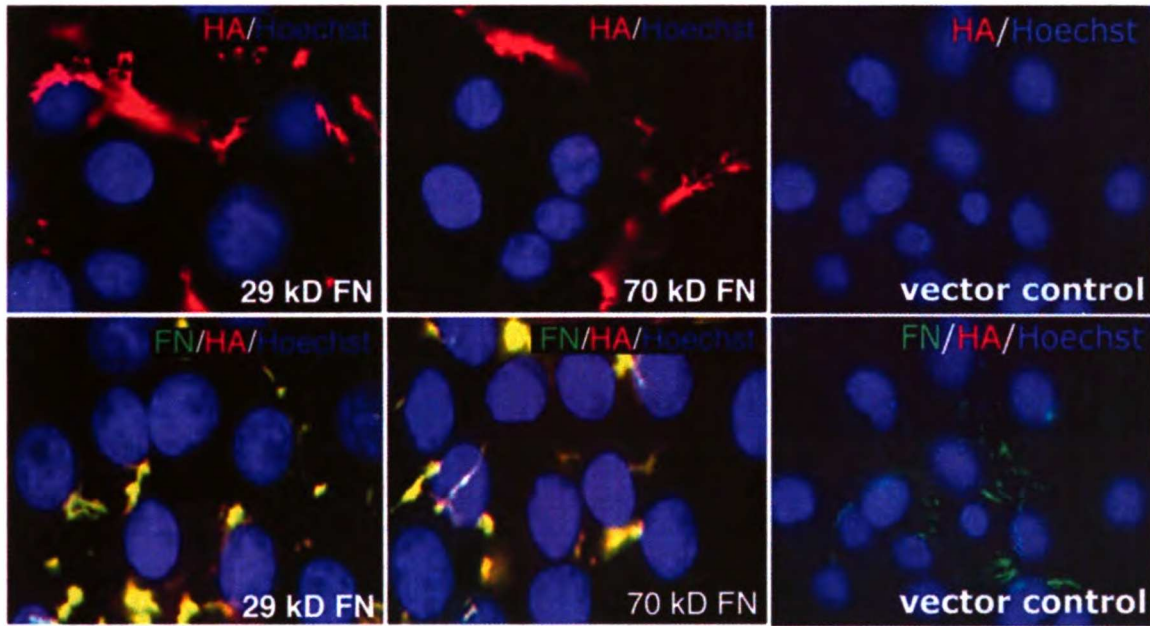


Figure 4. 29kD FN and 70kD FN transgene protein is secreted and incorporated into endogenous FN fibrillar matrix in ROS cells. Live ROS cells with stable integration of 29kD, 70kD FN transgene or empty control vector were stained with HA epitope tag antibody alone [top panel] or with HA antibody (red) and FN antibody (green) [lower panel]. Data show colocalization of 29kD FN or 70kD FN transgene protein with endogenous FN fibrillar matrix. Note the absence of staining with HA tag antibody in vector control ROS cells.

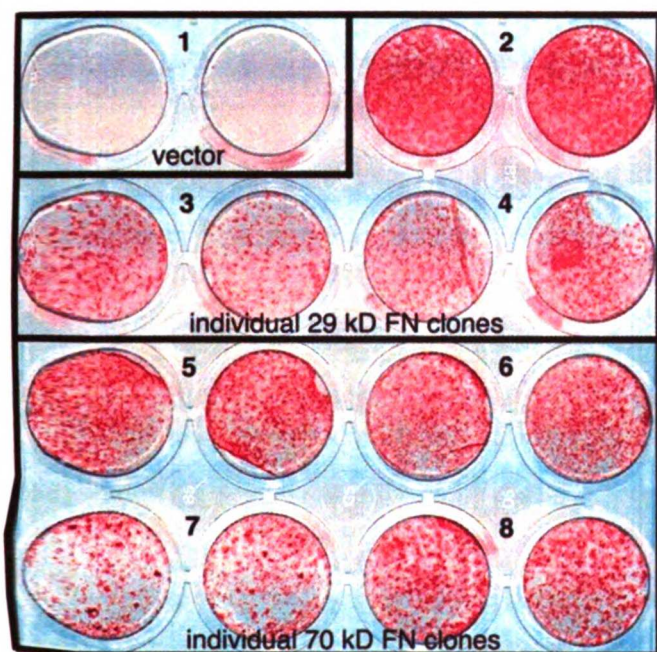


Figure 5. Increased matrix mineralization in ROS 17/2.8 osteosarcoma cells expressing 29kD FN or 70kD FN protein. Alizarin Red staining of 21-day ROS cell cultures in differentiation medium containing 100ug/ml Ascorbic Acid and 5mM β -glycerophosphate. The Alizarin Red stain reflects calcium deposition in the extracellular matrix and is an indicator of mineralization. Elevated red stain in the matrix of ROS cells expressing 29kD and 70kD FN suggests a positive impact of these FN domains on matrix mineralization.

Generation of 29kD and 70kD FN transgenic mice and characterization of transgene expression and localization in the bone.

Using the linearized transgene constructs, we established four independent transgenic founder lines of 29kD FN transgenic mice and five founder lines of 70kD FN transgenic mice, as shown by Southern blotting (partial data Figure 6) and by PCR analysis of genomic DNA isolated from mouse tails (data not shown). Expression of the 29kD FN and 70kD FN mRNA was evaluated by RT-PCR of the total RNA isolated from mouse femurs. Three out of the four 29kD FN transgenic lines (29kD FN line#01, 08 and 10) and four out of the five 70kD transgenic lines (70kD FN line# 24, 65, 76 and 85) expressed the transgene mRNA in bone, all at similar levels (Figure 7). Expression of the 29kD FN and 70kD FN proteins was assessed by western blotting of total calvarial protein extracts using an antibody for the C-terminal HA epitope tag (Figure 8). Two of the four 70kD FN transgenic lines, line 24 and line 65 (referred to as FN70-TG24 and FN70-TG65 in the following text), have detectable transgene expression at the protein level in the bone with TG65 at a higher level than TG24. None of the three 29kD FN transgenic lines had detectable levels of protein expression in the bone. Loss of the HA epitope tag or instability of the 29kD FN fragment in the bone could account for the failure to detect 29kD FN protein expression in the bone. To evaluate the transgene protein localization in the bone, we did immunohistochemistry staining on frozen saggital sections of D10 calvarial bones using a biotinylated anti-HA antibody (Figure 9). Positive immunoreactivity was pronounced on the bone surfaces in both FN70-TG24 and FN70-TG65 lines with osteocyte staining more prominent in the TG65 line. Again, there was no detectable staining on 29kD bone sections. Therefore, the 70kD FN expressing TG24 and

TG65 lines were followed for more extensive phenotypic analysis with an emphasis on TG65 due to its higher level of protein expression. Some aspects of phenotype characterization were also done with the 29kD FN transgenic mouse line 1 and 10 (FN29-TG01 and FN29-TG10). Therefore, for each aspect of phenotype characterization, I will present FN70-TG65 data first and then corroborate with supporting data from the FN70-TG24 line, and the FN29 lines TG01 and T10 where available. The 29kD FN transgenic mouse line 08 (FN29-TG08) had a unique and strong phenotype that was likely unrelated to the phenotype of any of the other lines. Thus, I will report data from TG 08 in a separate section at the end.

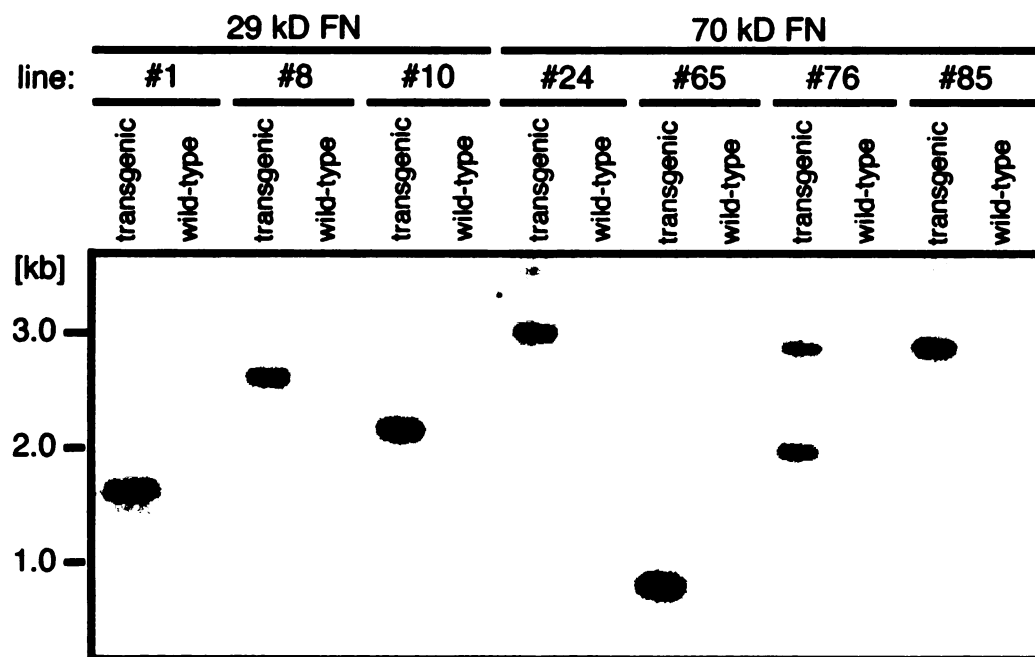


Figure 6. Identification of transgenic mice by Southern blot. EcoRI-restricted genomic DNA samples from PCR positive transgenic and PCR negative wild type mouse tails were size fractionated and hybridized to the 800bp probe for 29kD FN mouse lines (#01, 08 and 10)) and the 860bp probe for 70kD FN mouse lines (#24, 65, 76 and 85) (B). All lines used for further study (FN29TG01, FN29TG10, FN29TG08, FN70TG24, FN70TG65) contained a single integration site.

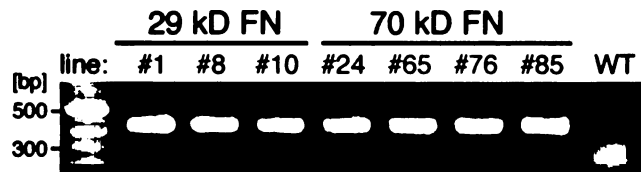


Figure 7. RT-PCR analysis of expression of the 29kD FN and 70kD FN transgene mRNA in bone RNA. PCR product was shown for mouse lines #1,8 and 10, which are **positive** for the 29kD FN transgene mRNA. PCR product was also shown for mouse lines #24, 65, 76 and 85, which are positive for the 70kD FN transgene mRNA. No PCR **product** was detected for a mouse that was negative for the transgene. Abbreviations: **WT**, wild type

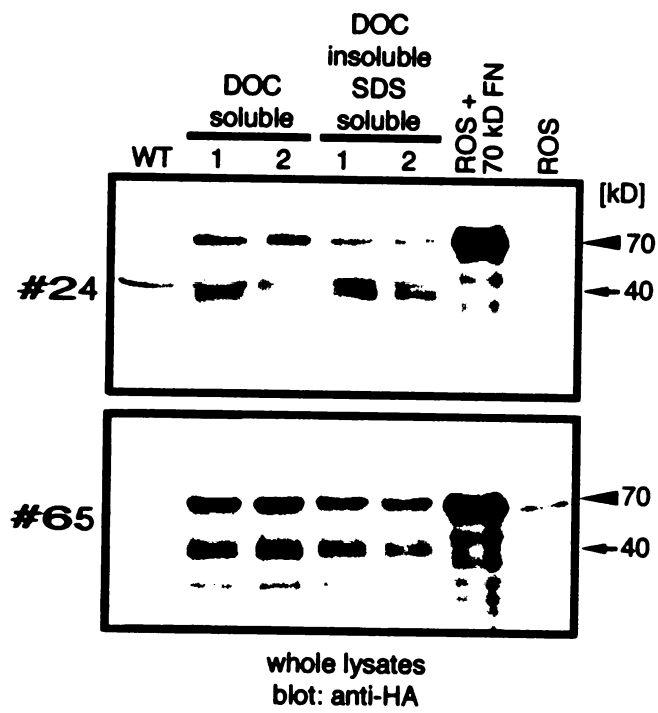
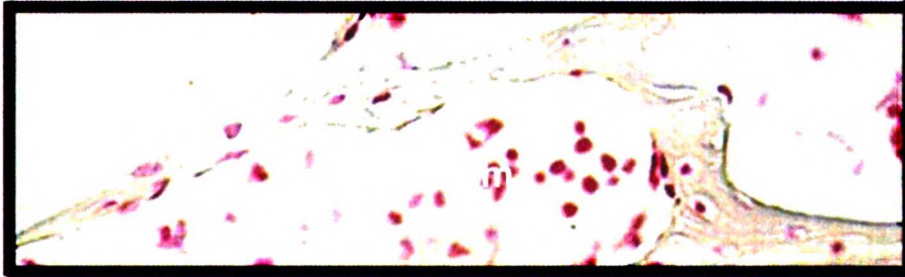
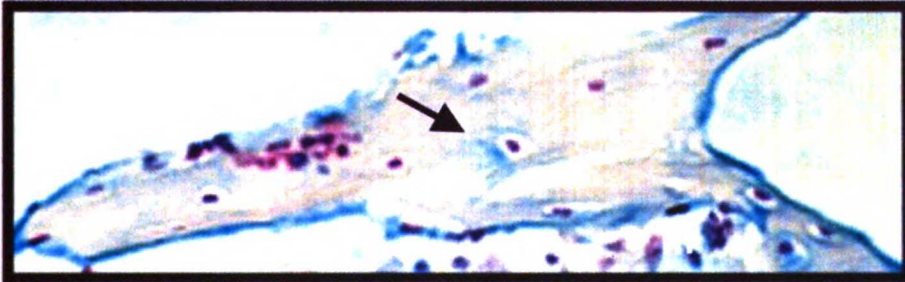


Figure 8. Western blot analysis of expression of the 70kD FN transgene protein in bone protein extracts. The skulls of two 10-day-old transgene-positive (1, 2) mice and one transgene-negative littermate (WT) each from 70kD FN line #24 and line #65 were dissected, minced and lysed sequentially in two kinds of detergent buffer. Each bone was first extracted with 2%DOC buffer to obtain DOC soluble supernatant fraction (DOC) and then the DOC insoluble precipitate was further extracted with 1% SDS buffer. 20ug protein lysate was used for detection with HA epitope tag antibody to recognize the 70kD FN transgene protein. 5ug lysate of ROS cells stably expressing the same transgene construct was used as a positive control. 5ug lysate of ROS cells stably expressing the empty control construct was used as negative control. A 70kD FN band (arrowhead) was detected in lysates of transgene-positive mouse bones in both the DOC-soluble and DOC-insoluble SDS-soluble fractions. This suggests that transgene protein was not only synthesized but also incorporated into an insoluble matrix. The absence of the 70kD band in lysates of wild type (WT) skulls verifies the specificity. Also, to note, a 40kD band (arrows) showed up in the transgene-positive lysates but not in the WT lysates. This is likely a degradation product of the 70kD FN protein.

WT



TG65



TG24

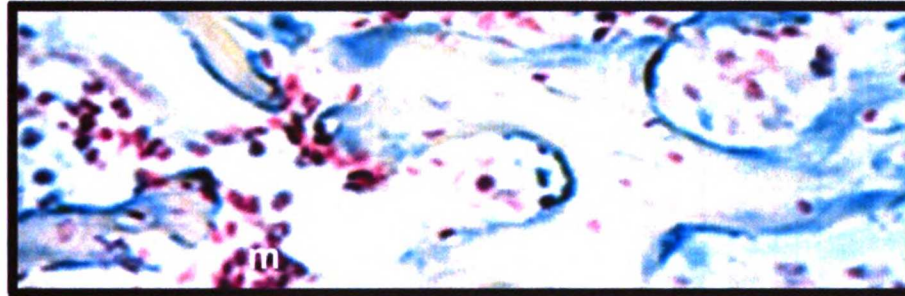


Figure 9. Expression and localization of 70kD FN transgene protein in the bone. Immunohistochemical staining of calvarial frozen sections from 10-day-old wild-type and transgene line #24 and #65 using HA epitope tag antibody to detect the 70kD FN transgene protein. The use of True blue as a substrate results in blue staining for 70kD FN. Sections were counterstained with Contrast red (Red). Transgenic bone showed strong 70kD FN immunoreactivity on the bone surfaces and in osteocytes (black arrow). Abbreviations: b, bone; m, bone marrow.

Phenotypic characterization of 29kD and 70kD FN transgenic mice

Macroscopic evaluation of the skeletal phenotype

Mice were evaluated for most parameters at D35 and D90. Transgenic mice in all lines except FN29-TG08 line appeared generally healthy. The mortality rate and fertility rate of transgenic mice were similar to wild type with the exception of TG24, which had some difficulty with mating and had two female mice die with abdominal tumors. All visceral organs appeared grossly normal after autopsy. Significant differences between wild type and transgenic mice in body weight and tibia bone length were observed at D35 with the body weight of two TG lines (TG65M, TG01F and TG01M) higher and two TG lines (TG24F and TG10F) lower, and the bone length of TG65M longer and TG24F shorter (table 1.1 and table 1.2.). Thus, there is no consistent correlation between body weight and transgene expression. However, a consistent positive correlation was found between bone length and body weight within each transgenic line. At D90, TG65 female mice had a slight, but significant increase in tibia bone length (1.5%, $p=0.0482$) though no difference in body weight ($p=0.8943$) (table 1.3. and table 1.4.). No significant difference of either body weight or tibia bone length was observed in male TG65 and other lines of mice. Similar trend of increased bone length in D90 female TG65 femora was also demonstrated by microCT bone length measurements showing that transgenic femora were longer than wild type femora (1%, $p=0.0724$: table 3.2). X-ray analyses of D35 (data not shown) and D90 male tibiae from transgenic mice did not show detectable differences in radio-opacity compared to those of the wild type mice (Figure 10). However, X-ray micrographs of D90 female transgenic tibiae showed higher radio-opacity of the diaphysis in all four lines examined (FN70-TG24 and FN70-TG65 and FN29-TG01 and

FN29-TG10) with TG24 having the smallest apparent difference from wild type among the four lines. We therefore focused our other aspects of phenotype characterization with female mice except when otherwise noted.

Table 1.1. D35 Mouse whole body weight statistics

	TG65F	TG65M	TG24F	TG24M	TG01F	TG01M	TG10F	TG10M
genotype	70kD	70kD	70kD	70kD	29kD	29kD	29kD	29kD
%Δ	+2%	+12.9%	-11.3%	-7.9%	+5.5%	+8.3%	-10.7%	-3.4%
p-Value	0.3698	0.0006	0.0083	0.0549	0.0353	0.0224	0.0147	0.4330

Table 1.2. D35 mouse tibia bone length statistics

	TG65F	TG65M	TG24F	TG24M	TG01F	TG01M	TG10F	TG10M
genotype	70kD	70kD	70kD	70kD	29kD	29kD	29kD	29kD
Δ	+0.02mm	+0.46mm	-0.49mm	-0.38mm	+0.21mm	+0.14mm	-0.24mm	-0.16mm
p-Value	0.8991	0.0008	0.0237	0.0861	0.1989	0.2815	0.2567	0.5009

A minimum of eight female and eight male mice from wild type and each of transgenic lines (FN29 lines TG01 and TG10; FN70 lines TG24 and TG65) was included in this study. Mice were sacrificed and weighed on an electronic scale. One tibia bone from each mouse was dissected free of soft tissues. Bone length was then measured by an electronic caliper with a resolution of 0.01mm and an accuracy of +/- 0.03mm. Abbreviation: F, female; M, male; % Δ , (mean TG weight – mean wild type weight / mean wild type weight) x 100; Δ , mean TG tibia bone length – mean wild type tibia bone length.

Table 1.3. D90 Mouse whole body weight statistics

	TG65F	TG65M	TG24F	TG24M	TG01F	TG01M	TG10F	TG10M
genotype	70kD	70kD	70kD	70kD	29kD	29kD	29kD	29kD
%Δ	-0.6%	-3.2%	-6%	-4.8%	+2.7%	+5.4%	-3.3%	-6%
p-Value	0.8943	0.4419	0.2161	0.2536	0.5497	0.2569	0.4461	0.1572

Table 1.4. D90 mouse tibia bone length statistics

	TG65F	TG65M	TG24F	TG24M	TG01F	TG01M	TG10F	TG10M
genotype	70kD	70kD	70kD	70kD	29kD	29kD	29kD	29kD
Δ	+0.19mm	-0.04mm	+0.05mm	-0.25mm	+0.16mm	+0.25mm	+0.03mm	-0.31mm
p-Value	0.0482	0.8389	0.6670	0.2040	0.0929	0.2561	0.7693	0.1125

A minimum of eight female and eight male mice from wild type and each of transgenic lines (FN29 lines TG01 and TG10; FN70 lines TG24 and TG65) was included in this study. Mice were sacrificed and weighed on an electronic scale. One tibia bone from each mouse was dissected free of soft tissues. Bone length was then measured by an electronic caliper with a resolution of 0.01mm and an accuracy of +/- 0.03mm. Abbreviation: F, female; M, male; % Δ , (mean TG weight - mean wild type weight / mean wild type weight) x 100; Δ , mean TG tibia bone length - mean wild type tibia bone length.

FEMALES

MALES

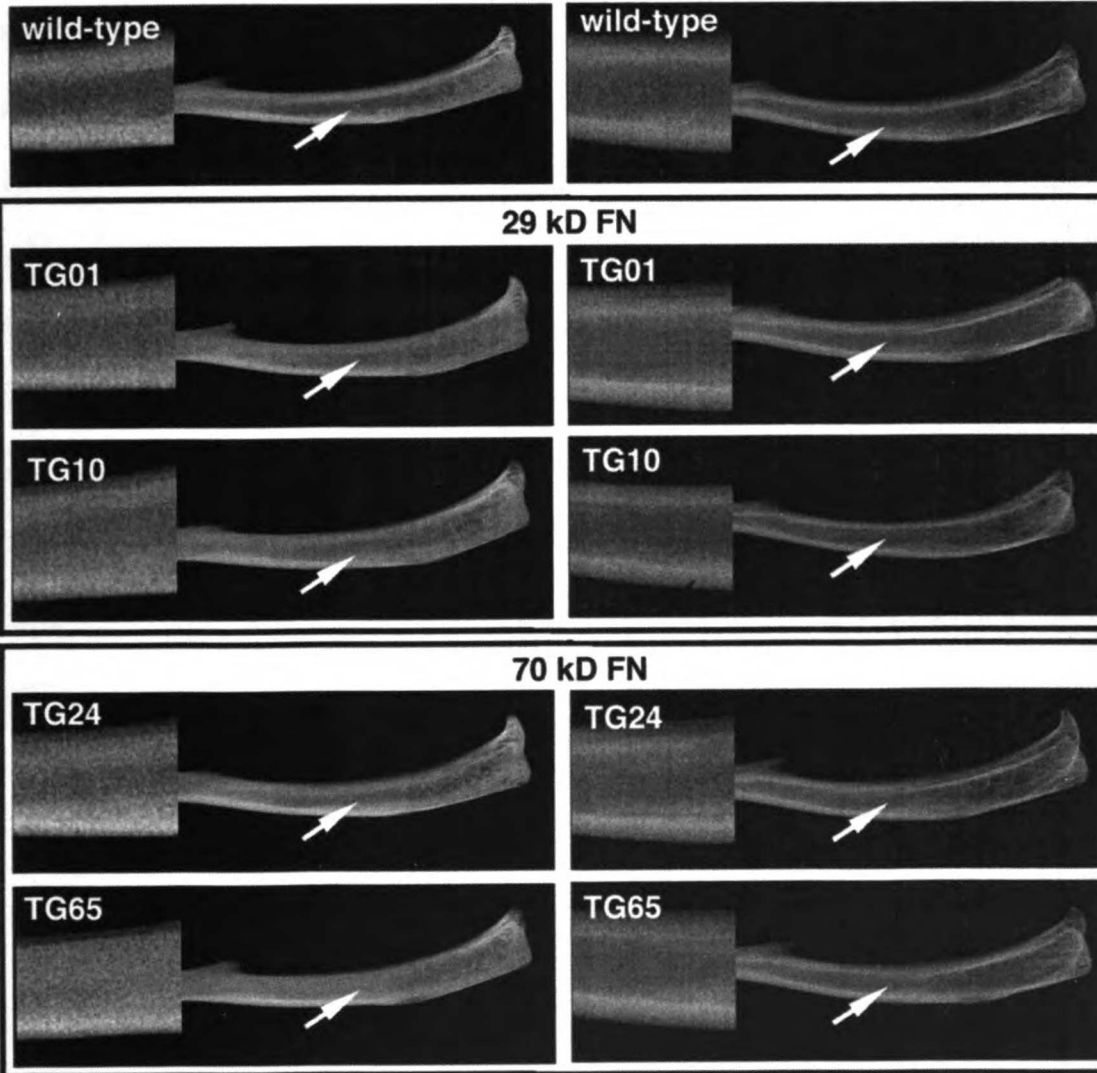


Figure 10. X-ray analysis of tibiae from D90 transgenic and wild type mice. Tibiae were dissected free of soft tissues. Frontal plane bone microradiographs were taken using Faxitron 43805N. Note the higher radio-opacity of the diaphysis in female transgenic bones from 29kD FN transgenic lines (TG01 and TG10) and 70kD FN transgenic lines (TG24 and TG65) compared to female wild type bones. Note the least difference in line TG24. No gross difference was present in the male bones. Representative X-ray images of one tibia from wild type and each transgenic mouse lines (TG01, TG10, TG24, TG65) were shown above. Tibiae from 8 female wild type, 8 female TG01, 9 female TG10, 6 female TG24 and 9 female TG65 mice were imaged on one X-ray film by faxitron. Tibiae from 7 male wild type and 8 male transgenic mice of each line were imaged on the other X-ray film by Faxitron.

Statistical analysis

For D35 phenotype analysis, wild type littermates were used as control mice. For D90 analysis using μ CT for bone volume and density and three-point bending test for biomechanical properties, both littermate and non-littermate wild type mice of the same strain were used. The need to use non-littermate wild type mice was due to the difficulty of obtaining wild type littermate controls after several generations of sibling mating. These non-littermate wild type mice were originally derived from F1 transgenic mouse matings and were bred and housed in the same facility. To address whether or not non-littermate wild type mice are suitable controls, one-factor ANOVA comparing wild type littermates to wild type non-littermates (Table 2.1) and also ANOVA comparing transgenic and wild type littermates (Table 2.2) was performed. There is no statistically significant difference between wild type littermates and non-littermates in the parameters used in the study. In addition, when data from non-littermate control mice were excluded from statistical tests, transgenic mice were still significantly different from littermate wild type mice for the same parameters, as they were when data from both littermate and non-littermate wild type were combined. Therefore, in assessing all data, littermate and non-littermate mice were analyzed as one control group when applying statistical analysis.

Table 2.1. Statistics comparing 4 wild-type littermates and 4 wild-type non-littermates

	Mean littermate	Mean non-littermate	ANOVA p value
BV/TV	0.59±0.02	0.60±0.01	0.6644
Marrow volume	1.97±0.17	2.00±0.23	0.8133
Cortex mineralization	17767±168	17819±129	0.6458
Failure Moment	23.17±2.85	25.41±2.10	0.2537
Stiffness	148.41±26.72	187.00±39.56	0.1570
Energy to failure	8.39±0.31	8.24±1.33	0.8361
Post-yield deformation	0.31±0.07	0.28±0.12	0.6723
Moment of inertia	0.20±0.06	0.13±0.04	0.1081

Table 2.2. Statistics comparing 9 TG65 and 4 wild-type littermates

	Mean littermate	Mean TG65	ANOVA p value
BV/TV	0.59±0.02	0.64±0.04	0.0243
Marrow volume	1.97±0.16	1.74±0.228	0.0581
Cortex mineralization	17767±17	17984±161	0.0206
Failure Moment	23.17±2.85	31.31±5.94	0.0262
Stiffness	148.40±26.72	281.08±98.99	0.0256
Energy to failure	8.39±0.31	6.57±1.52	0.0410
Post-yield deformation	0.31±0.07	0.12±0.09	0.0045
Moment of inertia	0.20±0.06	0.34±0.07	0.0062

Transgenic cortical bone matrix is more disorganized

To assess the integrity and structure of bone matrix, transgenic and wild type tibiae were analyzed histologically at D14 and D35 and femora at D90. Longitudinal sections through the proximal tibia from D14 and D35 wild type and FN29-TG01, TG10, and FN70-TG65 mice were stained with Trichrome (Figure 11, partial data shown for TG65 only). No gross difference in the trabeculation of the metaphysis or in the appearance of the epiphysis were observed in multiple sections examined throughout the bone.

Longitudinal sections of the tibiae from D35 (Figure 12) and the femora from D90 (Figure 13) wild type and FN70-TG65 mice were further analyzed for the organization of the bone matrix. Sections were stained with H&E and viewed by transmitted or polarized light microscopy. At D35 and D90, the skeleton is mature with the conclusion of the period of rapid bone formation and growth. Thus, the vast majority of bone matrix present should be in a mature lamellar form with highly ordered parallel collagen fibers that can be visualized by polarized light (Figure 12). In comparison to lamellar bone, areas of woven bone are characterized by a lighter pink stain, irregular nuclei orientation and a generally higher cell density when viewed by bright field transmitted light microscopy, as delimited by the yellow line. The polarized light image of such areas showed either scarce collagen fibers and/or irregular collagen fiber orientation. Quantification of the area of woven bone in the mid-diaphysis normalized by total bone area analyzed revealed 11% for the wild type and 27% for the transgenic bones at D35 ($p=0.0324$), and 9% for the wild type and 19% for the transgenic bones at D90 ($p=0.0091$). In addition, D90 transgenic bones have significantly higher number of

tunnel-like structure perpendicular to the parallel lamellar structure ($p=0.0073$). The identity of this tunnel-like structure is not clear. These observations suggested that compared to wild type, the cortical bone matrix of the FN70-TG65 bones is more disorganized indicating accelerated ECM deposition and/or defective or delayed ECM maturation. This matrix organization phenotype in the cortex prompted us to look further into the cortical bone thickness and volume, bone mineralization and cortical bone density, whole bone structural strength and cortical bone tissue level material properties.

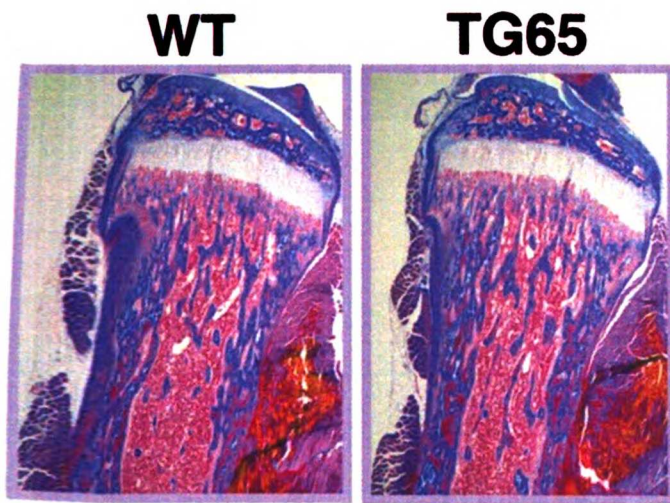


Figure 11. Histological appearance of transgenic bone. Longitudinal sections through the proximal tibiae of D35 wild type and FN70-TG65 mice. The Aniline Blue (AB) component of the trichrome stains the bone blue. There is no gross difference in the trabeculation of the metaphysis or in the appearance of the epiphysis.

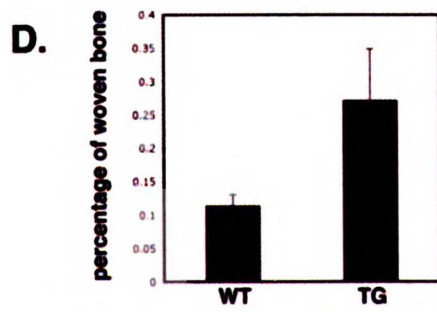
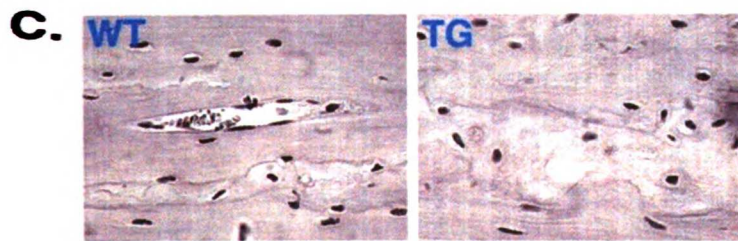
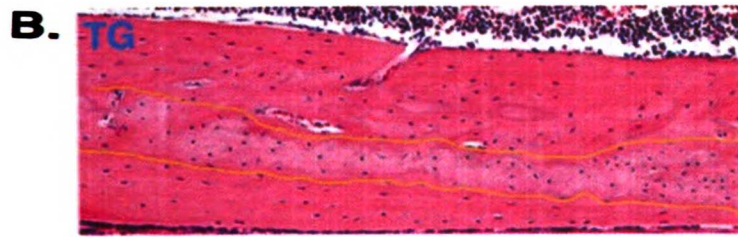
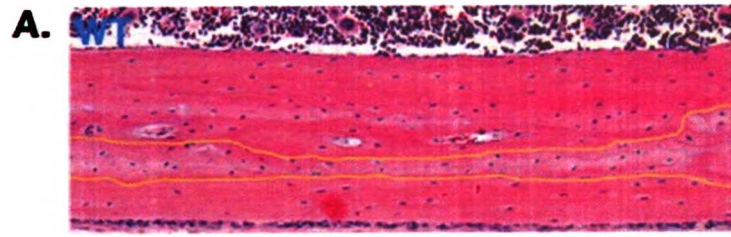


Figure 12. Transgenic cortical bone matrix is more disorganized at D35. Longitudinal sections of the cortical bone in the diaphysis of the tibia from D35 wild type and transgenic mice were stained with H & E. In comparison to lamellar bone, the non-lamellar bone is characterized by lighter pink stain and irregular orientation of nuclei, and is delimited by the yellow line (A, B). Polarized light image of this area showed a lower density of collagen fibrils and more irregular collagen fiber orientation (C). Abbreviation: c, cortex; m, bone marrow. Cortical bone in both wild type and transgenic mice showed areas of woven or lamellar structure. Fractional area of woven bone was determined using Photoshop image analysis software. A total of 6 wild-type and 7 transgenic bones from 35-day old mice were analyzed in this study. Quantification of the area of woven bone versus total bone area showed that transgenic mice cortical bone has significantly higher portion of woven bone compared to wild type ($p=0.0324$) (D).

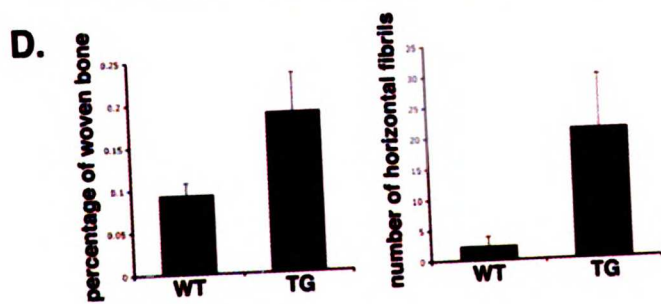
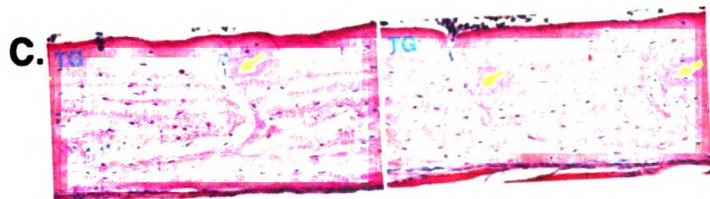
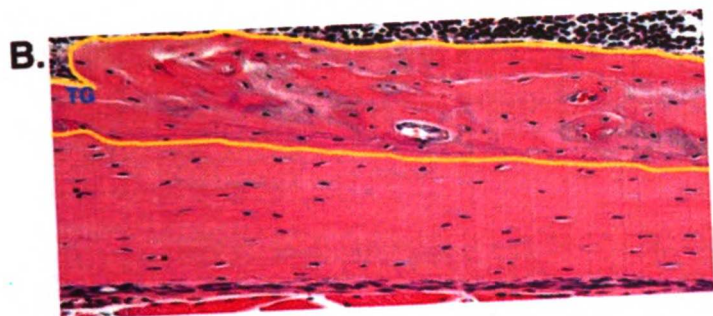


Figure 13. Transgenic cortical bone matrix is more disorganized and has significantly higher number of tunnel-like structure perpendicular to the parallel lamellae at D90. Longitudinal sections of the cortical bone in the diaphysis of the femur from D90 wild type and transgenic mice were stained with H & E. The woven bone is delimited by the yellow line (A, B). Note the irregularity of the endosteal surface and the endocortical woven bone (B) and the tunnel-like structure perpendicular to the parallel lamellae (arrow in C) in transgenic cortex. Quantification of the area of woven bone versus total bone area showed that transgenic mice cortical bone has significantly higher amount of woven bone compared to wild type ($p=0.0091$) (D, left graph). The number of vertical tunnel-like structure was quantified from three longitudinal sections 300 μm apart each bone. A total of 5 wild type and 5 transgenic bones from 90-day-old mice were analyzed in this study. Transgenic bones have significantly more vertical channel-like structure than wild type bones ($p=0.0073$) (D, right graph).

Transgenic femoral bone is greater in cortical bone thickness and volume

To determine the impact of 70kD FN expression on cortical bone thickness and volume, mid-diaphysis of the femora from female wild type, FN70-TG24 and FN70-TG65 mice were analyzed by quantitative micro-computed tomography (μ CT in collaboration with Dr. Ellen Filvarof (*Genentech*) (Table 3.1 and Table 3.2), and mid-diaphyseal geometry of the femora from wild type and all four transgenic mouse lines (FN29-TG01, FN29-TG10, FN70-TG24, FN70-TG65) were obtained from two-axis X-ray microradiograph images (Table 4.1 and Table 4.2). FN70-TG65 μ CT analysis of both D35 and D90 transgenic mice showed an increase in cortical bone thickness and volume compared to wild type mice (Table 3.1 and Table 3.2). Specifically, compared to wild type femoral cortical bones, transgenic cortex was 12% thicker ($p < 0.0001$) at D35 and 8% thicker ($p = 0.0094$) at D90; transgenic cortical bone volume was 18% greater ($p = 0.0002$) and 6% greater ($p = 0.0784$) at D90; transgenic bone total tissue volume was 9% greater ($p = 0.0121$) at D35 and no significant difference at D90; percentage of cortex volume normalized by tissue total volume was 7.9% bigger ($p < 0.0001$) at D35 and 7.6% bigger ($p = 0.0089$) at D90; transgenic bone marrow volume was not significantly different at D35, yet 12% smaller ($p = 0.0290$) at D90. The D90 TG65 female μ CT parameters are also presented in a histogram plot (Figure 14) illustrating that more transgenic mice are in the higher data range of cortical bone volume and bone density, yet in a lower data range of marrow volume, than wild type mice. Taken together, on and before D35, 70kD FN transgene expression in mouse bones leads to positive effects on cortical bone thickness and volume by increasing cortex volume and total tissue volume, while maintaining similar marrow volume. This suggests that 70kD FN expression in bone regulates bone

modeling by either increasing bone formation or decreasing bone resorption at the periosteal surface of the cortex during the period of pre-pubertal rapid bone modeling and bone growth. On the other hand, between D35 and D90, 70kD FN transgene expression in mouse bones exerts a positive effect on cortical bone thickness and volume by increasing cortex volume, decreasing marrow volume while maintaining similar total tissue volume. This indicates that 70kD FN expression regulates bone remodeling by either increasing bone formation or decreasing bone resorption at the endosteal surface of the cortex during the period of bone remodeling and adult bone growth.

Supporting data of the positive effect of transgene expression on cortical bone thickness are also provided from D90 femoral diaphyseal geometry measurements using two axis X-ray microradiographs (table 4.1 and table 4.2). Major outer diameter, minor outer diameter, major inner diameter and minor inner diameter of the mid-diaphysis were direct measurements from the X-ray image. Major cortex thickness, minor cortex thickness and moment of inertia were calculated from these four parameters. Major and minor outer diameters were significantly bigger in FN70-TG65, FN29-TG01 and FN29-TG10 female and male transgenic femurs in comparison with wild type control femurs. Minor inner diameter was significantly smaller in FN70-TG65, FN29-TG01 and FN29-TG10 female but not male transgenic femurs. There was no difference in the major inner diameters in these three transgenic lines. Overall, when compared with wild type mice, the major and minor cortex thickness and moment of inertia were significantly bigger in TG65, TG01 and TG10 ($p < 0.01$). However, D90 FN70-TG24 did not show a similar trend by either geometry measurements or μ CT analysis. Instead, by geometry measurements, D90 TG24

femora had a slight decrease in minor diameter in males and an increase in major and minor inner diameter in females and, no difference in cortex thickness. In addition, μ CT analysis suggested that D90 TG24 femora have a slight decrease in cortical bone thickness ($p=0.048$) in the females especially from the periosteal side. However, there is no significant difference in bone volume (BV) normalized to total tissue volume (TV) in this TG line (data not shown). Considering the fact that the weight of the female TG24 mice was statistically less than that of the wild type mice ($p=0.036$), the slight decrease in cortical bone thickness may be due to lighter weight. Thus both μ CT and geometry data point to a greater cortical bone thickness and volume phenotype in three transgenic mouse lines, FN70-TG65 and FN29-TG01 and TG10. Therefore, transgenic femurs from these lines would be expected to show greater whole bone strength if the local material mechanical properties are the same.

Table 3.1. FN70-TG65 D35 female mice show an increase in femoral cortical bone volume by μ CT analysis (Mean \pm SD)

genotype	N	Total Volume (mm ³)	Cortex Volume (mm ³)	Cortex Thickness (mm)	Marrow Volume (mm ³)	BV/TV	Bone Length (mm)
WT	9	3.35 \pm 0.27	1.52 \pm 0.14	0.12 \pm 0.01	1.85 \pm 0.14	0.45 \pm 0.01	11.51 \pm 0.33
TG65	8	3.67 \pm 0.16	1.79 \pm 0.07	0.13 \pm 0.00	1.89 \pm 0.11	0.49 \pm 0.01	12.06 \pm 0.13
$\Delta\%$		+9.3	+17.9	+11.8	+2.3	+7.9	+4.8
p-Value		0.0121	0.0002	<0.0001	0.5064	<0.0001	0.0005

Table 3.2. FN70-TG65 D90 female mice show an increase in femoral cortical bone volume by μ CT analysis (Mean \pm SD)

genotype	N	Total Volume (mm ³)	Cortex Volume (mm ³)	Cortex Thickness (mm)	Marrow Volume (mm ³)	BV/TV	Bone Length (mm)
WT	8	4.83 \pm 0.34	2.87 \pm 0.18	0.18 \pm 0.00	1.98 \pm 0.19	0.59 \pm 0.02	14.21 \pm 0.21
TG65	9	4.75 \pm 0.18	3.03 \pm 0.18	0.19 \pm 0.01	1.74 \pm 0.23	0.64 \pm 0.04	14.36 \pm 0.07
$\Delta\%$		-1.7	+5.7	+7.9	-12.4	+7.6	+1.0
p-Value		0.5276	0.0784	0.0094	0.0290	0.0089	0.0724

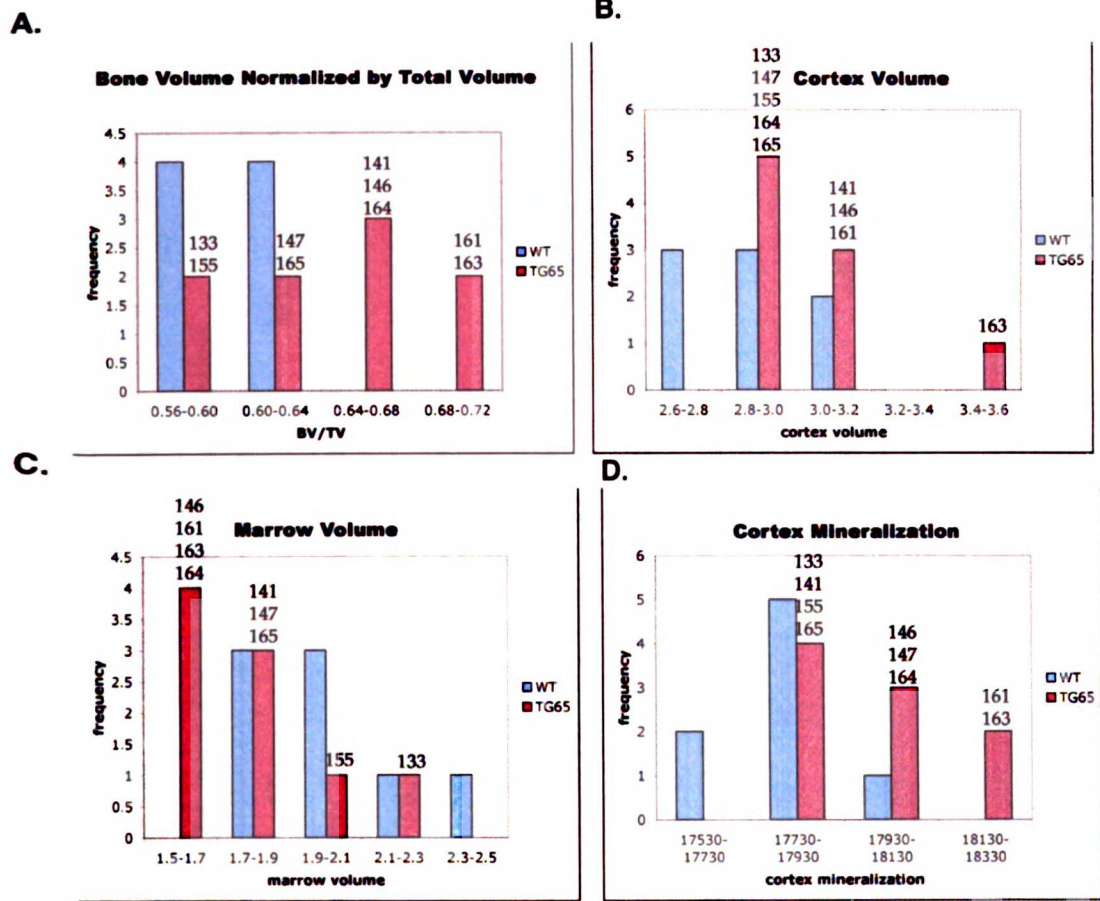


Figure 14. Histogram plot of microCT measurements of female bones at 90 day old. The X-axis shows ranges of Bone Volume normalized to total Tissue Volume (A), Cortex Volume (B), Marrow Volume (C), and Cortex Mineralization (D). The Y-axis shows the number of mice in each range. In the graph, wild type is blue; transgenic is red. The unique ID number of each transgenic mouse is also shown on the graph. This graph illustrates that more transgenic mice are in the higher data range of bone volume and bone density, yet in the lower data range of marrow volume, than wild type mice.

Table 4.2. Geometry measurements of femoral cortical bone from D90 FN29-TG01, FN29-TG10, FN70-TG24, and FN70-TG65 male mice

	Major Diameter	Minor Diameter	Major Inner Diameter	Minor Inner Diameter	Major Cortex thickness	Minor Cortex thickness	Minor Moment of Inertia
WT	1.57±0.09	1.27±0.05	1.16±0.06	0.96±0.04	0.21±0.11	0.16±0.07	0.19±0.04

	Major Diameter	Minor Diameter	Major Inner Diameter	Minor Inner Diameter	Major Cortex thickness	Minor Cortex thickness	Minor Moment of Inertia
TG01	1.88±0.06	1.48±0.04	1.10±0.05	0.80±0.03	0.39±0.07	0.34±0.07	0.45±0.06
Δ	+	+			+	+	+
p-value	0.0016	0.0057	0.50	0.064	0.0031	0.0012	0.0001

Table 4.2. (continued)

	Major Diameter	Minor Diameter	Major Inner Diameter	Minor Inner Diameter	Major Cortex thickness	Minor Cortex thickness	Moment of Inertia
TG10	1.83±0.05	1.41±0.05	1.20±0.04	0.89±0.03	0.31±0.05	0.26±0.05	0.35±0.02
Δ	+	+			+	+	+
p-value	0.0035	0.033	0.57	0.35	0.0237	0.0046	0.0034

	Major Diameter	Minor Diameter	Major Inner Diameter	Minor Inner Diameter	Major Cortex thickness	Minor Cortex thickness	Moment of Inertia
TG24	1.68±0.03	1.16±0.03	1.23±0.07	0.91±0.07	0.23±0.08	0.15±0.07	0.17±0.02
Δ							
p-value	0.20	0.088	0.36	0.54	0.3666	0.4278	0.77

Table 4.2. (continued)

	Major Diameter	Minor Diameter	Major Inner Diameter	Minor Inner Diameter	Major Cortex thickness	Minor Cortex thickness	Moment of Inertia
TG65	1.96±0.04	1.46±0.05	1.26±0.03	0.99±0.04	0.35±0.05	0.24±0.06	0.45±0.04
Δ	+	+			+	+	+
p-value	0.0001	0.0043	0.16	0.67	0.0064	0.0195	0.0001

X-ray images of femora from 7 male wild type and 8 male transgenic mice of each line (TG01, TG10, TG24 and TG65 were taken in the anterior-posterior and medial-lateral planes and the two axis dimensions of the femoral diaphysis were measured at both the periosteal (major and minor diameter) and endosteal surfaces (major and minor inner diameter). These dimensions were used to calculate major and minor cortex thickness and the area moment of inertia (I , mm⁴). Abbreviations: WT, wild type; Δ, difference of measurements between transgene and wild type femora; +, significant increase; p-value, significance between transgene and wild type femora. Note the significant increase in Major and Minor Diameter, Major and Minor Cortex thickness and moment of inertia of the ale TG01, TG10 and TG65 femora in comparison to those of WT.

Transgenic femoral bone is greater in cortical bone density and bone mineralization

To determine the impact of transgene expression on cortical bone density, mid-diaphyseal cortex of femora from female FN70-TG24 and TG65 mice were analyzed by quantitative micro-computed tomography (μ CT). To examine the effect of transgene expression on bone mineral content and bone mineralization, tibiae from FN70-TG24, TG65 and FN29-TG01 and TG10 were analyzed by ash mass assay (in collaboration with Dr. Ruth Globus, NASA Ames Research Center). Measurement of bone mineral density (BMD) by μ CT revealed a small yet significant increase (1.1%, $p < 0.01$) in cortical BMD in femora of the TG65 mice, but not the TG24 mice, compared with wild type controls at both D35 and D90 (Table 5.1 and Table 5.2.). In addition, D 35 TG65 tibiae ash assay indicates a positive effect of transgene expression on bone mineral content and bone mineralization. Specifically, at D35, both bone ash mass and ash mass normalized to body mass (Ash/Body) are higher by 18.2% and 6.5% respectively ($p < 0.05$), in the transgenic mice compared to wild type mice. Bone dry mass and dry mass normalized to body mass (Dry/Body) are also higher by 11.1% and 4.8% respectively, in the transgenic mice compared to wild type mice. Yet, the difference is not statistically significant. In addition, ash fraction (Ash/Dry) is 3.2% higher ($p = 0.0369$) in the transgenic mice compared to wild type mice. Bone ash mass assay in TG01 and TG10 also shows a similar trend as TG65 in that both Ash/Body and Ash Fraction were increased, although not always showing statistical significance (Table 6.1-4). Specifically, tibia bone Ash/Body was higher in D35 female TG01 (9.72% increase, $p = 0.0015$) and in D90 male TG01 (8.48% increase, $p = 0.0221$) and D90 male TG10 (6.75% increase, $p = 0.0412$). In addition, tibia bone ash fraction was higher in D35 female TG10 (8.45% increase,

Table 5.1. FN70-TG65 D35 female mice show an increase in femoral cortical bone density by μ CT analysis and bone mineral content by bone ash assay (Mean \pm SD)

genotype	Body Mass (g)	μ CT cortical BMD (g-HA/cm ³)	Ash Mass (mg)	Ash/Body Mass (mg/g)	Dry Mass (mg)	Dry/Body Mass (mg/g)	Ash fraction
WT(n=9)	18.51 \pm 1.14	1.758 \pm 0.017	0.011 \pm 0.001	0.617 \pm 0.044	0.018 \pm 0.002	0.992 \pm 0.070	0.622 \pm 0.014
TG65(n=8)	18.93 \pm 0.61	1.777 \pm 0.017	0.013 \pm 0.001	0.663 \pm 0.031	0.020 \pm 0.001	1.040 \pm 0.045	0.638 \pm 0.021
$\Delta\%$	+2.2	+1.096	+18.2	+6.5	+11.1	+4.8	+3.2
p-Value	0.3698	0.0339	0.0354	0.0109	0.1194	0.1018	0.0369

Table 5.2. FN70-TG65 D90 female mice show an increase in femoral cortical bone density by μ CT analysis and bone mineral content by bone ash assay (Mean \pm SD)

genotype	Body Mass (g)	μ CT cortical BMD (g-HA/cm ³)	Ash Mass (mg)	Ash/Body Mass (mg/g)	Dry Mass (mg)	Dry/Body Mass (mg/g)	Ash fraction
WT(n=8)	24.165 \pm 1.435	1.913 \pm 0.015	0.017 \pm 0.001	0.689 \pm 0.041	0.024 \pm 0.001	0.998 \pm 0.059	0.691 \pm 0.013
TG65(n=9)	24.026 \pm 1.157	1.934 \pm 0.017	0.017 \pm 0.001	0.706 \pm 0.068	0.024 \pm 0.002	1.018 \pm 0.093	0.693 \pm 0.013
$\Delta\%$	-0.8	+1.074	0	+2.899	0	+2.0	0
p-Value	0.8686	0.0206	0.5135	0.5489	0.6594	0.5872	0.8085

Abbreviation: $\Delta\%$, (TG measurement – WT measurement / WT measurement) x100

Table 6.1. Tibia bone mineral content from D35 female transgenic mice in comparison with that from the wild-type mice

Line	Ash/Body Wt. (mg/g)				Ash Fraction (mg/g)			
	TG01	TG10	TG24	TG65	TG01	TG10	TG24	TG65
$\Delta\%$	+9.72	-1.8	+2.8	+6.5	+1.3	+2.9	+2.6	+3.2
p-Value	0.0015	0.5215	0.3129	0.0109	0.2577	0.2143	0.2697	0.0369

Table 6.2. Tibia bone mineral content from D35 male transgenic mice in comparison with that from the wild-type mice

Line	Ash/Body Wt. (mg/g)				Ash Fraction (mg/g)			
	TG01	TG10	TG24	TG65	TG01	TG10	TG24	TG65
$\Delta\%$	+2.7	+4.2	+2.6	+2.8	+3.2	+8.45	+1.0	+1.7
p-Value	0.5963	0.2747	0.4790	0.4864	0.3367	0.0382	0.8033	0.5963

Table 6.3. Tibia bone mineral content from D90 female transgenic mice in comparison with that from the wild-type mice

Line	Ash/Body Wt. (mg/g)				Ash Fraction (mg/g)			
	TG01	TG10	TG24	TG65	TG01	TG10	TG24	TG65
$\Delta\%$	+4.6	+5.4	+4.6	+2.5	+0.6	+0.3	+0.6	+0.3
p-Value	0.2758	0.2027	0.3237	0.5489	0.7063	0.8222	0.6861	0.8085

Table 6.4. Tibia bone mineral content from D90 male transgenic mice in comparison with that from the wild-type mice

Line	Ash/Body Wt. (mg/g)				Ash Fraction (mg/g)			
	TG01	TG10	TG24	TG65	TG01	TG10	TG24	TG65
$\Delta\%$	+ 8.48	+6.75	+3.2	+4.8	+4.0	+3.1	+0.6	+4.0
p-Value	0.0221	0.0412	0.0913	0.1381	0.1016	0.1429	0.7372	0.1560

Transgenic tibiae show increased endocortical bone formation

Greater cortical bone mass phenotype is further confirmed by quantitative **histomorphometry** of the cortical bone of D90 mouse distal tibiae. Bone **histomorphometric** analysis was done in collaboration with Dr. Thomas Wronski at the **University of Florida**. 70kD FN mice had a higher cortical bone thickness and area than **the wild type control** (Table 7.1.). No significant difference in marrow area was detected **here**. However, μ CT showed a significant reduction in marrow volume in transgenic **femora** compared to wild type femora. A 20% of total bone length in the mid-diaphysis **of the** femora was analyzed with μ CT. Only one cross-section from each animal was used **for histomorphometry** analysis. Thus, histomorphometry data is a lot less representative **of the** entire bone than μ CT.

This phenotype of the 70kD FN mice suggested an imbalance between the rates of **osteoblastic** bone formation and osteoclastic bone resorption. The rate of bone deposition **can be** measured histomorphometrically from bone sections of mice injected sequentially **with** two fluorochrome labels that incorporate into bone matrix at sites of mineralization (Parfitt, 1983).

Comparison of 70kD FN and wild type cortical bone, using the D90 distal tibiae, **indicated** that the endocortical mineralizing surface per bone surface was 30% higher in **transgenic** mice though not statistically significant. This suggests that the percentage of **bone surface** undergoing formation was not significantly different. However, the

endocortical mineral apposition rate was 30% higher in D90 70kD FN tibiae (p=0.01). Multiplying the mineralizing surface per bone surface and the mineral apposition rate reveals a two-fold higher rate of endocortical bone formation per unit bone surface in 70kD FN mice compared to wild-type mice (p=0.02). In contrast, both the percentage of bone surface undergoing formation and the rate of bone formation at the periosteal bone surface were similar in 70kD FN mice compared to wild type mice. Osteoblast and osteoclast surface and the rate of osteoclastic resorption cannot be directly measured from the cross-sections of the tibiae.

Measurements of trabecular bone parameters in D90 70kD FN and wild type lumbar vertebrae and in distal femoral metaphyses 0.5 to 2.0 mm proximal to the growth plate did not reveal any significant differences (Table 7.2. and Table 7.3.). Cellular and fluorochrome endpoints were not measured in the distal femoral metaphyses because of low trabecular bone volume in this area.

In summary, histological, structural and histomorphometric studies show that transgenic mice have higher fraction of cortical woven bone, higher rate of endocortical bone formation and increased cortical bone volume and density compared to wild type mice. The question remains as to how these morphological and structural changes affect the functional integrity of the whole bone. To address this question, further experiments were carried out to examine the whole bone mechanical properties and bone tissue level material mechanical properties.

Table 7.1. FN70-TG65 D90 female mice show an increase in cortical bone volume and endocortical bone formation rate in distal tibiae by Histomorphometry analysis (Mean±SD)

N	Total tissue area (mm ²)	Cortical area (mm ²)	Marrow area (mm ²)	Cortical thickness (µm)	Periosteal MS/BS (%)	Periosteal MAR (µm/day)	Endocortical MS/BS (%)	Endocortical MAR (µm/day)	Endocortical BFR/BS (µm ³ /µm ² /day)
WT	10	0.93±0.10	0.62±0.03	0.31±0.09	227±22	6.4±4.6	20.7±17.7	0.9±0.2	0.17±0.22
TG65	11	0.93±0.08	0.66±0.03	0.27±0.07	244±18	9.6±14.3	32.4±18.6	1.2±0.2	0.36±0.18
p-Value		0.45	0.01	0.14	0.03	0.3	0.1	0.01	0.02

Abbreviations: total tissue area, cortical bone + bone marrow; Periosteal MS/BS, periosteal mineralizing surface (percentage of bone surface with demeclocycline label); Periosteal mineral apposition rate (distance between demeclocycline label and periosteal surface/13 days); Endocortical MS/BS, endocortical mineralizing surface (percentage of bone surface with both calcein labels); Endocortical MAR, endocortical mineral apposition rate (interlabel distance between the calcein label and 2nd calcein label/4 days); Endocortical BFR, endocortical bone formation rate(multiplying mineralizing surface by mineral apposition rate).

Table 7.2. FN70-TG65 D90 female mice do not show significant difference in trabecular bone volume and bone formation rate in lumbar vertebrae by Histomorphometry analysis (Mean±SD)

	N	BV/TV(%)	Tb.N (#/mm)	Tb.Th (µm)	Tb.Sp (µm)	Oc.S (%)	Ob.S (%)	MS/BS (%)	MAR (µm/day)	BFR/BS (µm ³ /µm ² /day)
WT	12	10.1±1.5	4.7±0.7	25.9±3.6	193.3±28.6	1.2±0.5	16.0±5.7	8.8±4.2	1.8±0.3	0.17±0.06
TG65	13	10.4±2.9	4.9±0.6	25.3±6.3	185.3±26.6	1.5±0.7	17.7±6.0	11.3±3.7	1.7±0.2	0.20±0.06
p-Value		0.4	0.3	0.4	0.2	0.2	0.2	0.1	0.3	0.14

Abbreviations: BV/TV, trabecular bone volume as a percentage of bone tissue area; Tb. N, trabecular number; Tb. Th, trabecular thickness; Tb. Sp, trabecular separation; Oc.S, osteoclast surface as a percentage of total trabecular bone surface; Ob.S, osteoblast surface as a percentage of total trabecular bone surface; MS/BS, mineralizing surface (percentage of trabecular bone surface with double calcein label plus single calcein label); MAR, mineral apposition rate; BFR, bone formation rate (MSxMAR)

Table 7.3. FN70-TG65 D90 female mice do not show significant difference in trabecular bone volume in distal femoral metaphyses 0.5 to 2.0 mm proximal to the growth plate by Histomorphometry analysis (Mean±SD)

	N	BV/TV(%)	Tb.N (#/mm)	Tb.Th (µm)	Tb.Sp (µm)
WT	12	5.5±1.8	2.8±0.7	23.4±4.7	354.3±90.0
TG65	13	5.1±1.4	2.5±0.5	24.3±4.7	395.6±78.9
p-Value		0.3	0.3	0.1	0.1

Transgenic femoral bone is weaker and less ductile in biomechanical strength

To determine whether the cortical bone histological and structural changes in transgenic mice were accompanied by structural strength differences, biomechanical properties of the femoral cortical bones from D90 FN70-TG65 (Table 8), FN70-TG24, FN29-TG01 and FN29-TG10 (Table 9 and Table 10) and wild-type mice were measured in a three-point bending test (in collaboration with Dr. Marjolein Van Der Meulen, Department of Mechanical Engineering, Cornell University). A schematic view of the load-displacement curve is shown in Figure 15. FN70-TG65 female, but not male femora had significantly higher failure moment (M_f) and maximum moment (M_m) than did wild type femora. TG65 femora also had higher stiffness (EI) than did wild type femurs with statistical significance only in the female mice. This higher whole bone structural strength in D90 female TG65 femora is consistent with the increased cortical thickness, volume and mineral density and increased cross-sectional size (moment of inertia) in this line, as described above. Nevertheless, when EI measurements were normalized by bone cross-sectional size (I , moment of inertia), EI/I , now named tissue modulus, they were 26% lower in female and 48% lower in male transgenic femora compared to wild type femora, though these differences were not statistically significant. In addition, both male and female FN70-TG65 femora had lower energy to failure (20% decrease) than did wild type femora, though statistically significant only in the females ($p=0.0392$). These findings indicate that long bones of FN70-TG65 were weaker than their wild type counterparts when bone geometry is not factored in. Post-yield deformation was also reduced in both female (60% decrease) and male (40% decrease) FN70-TG65, statistically significant only in females ($p=0.0048$), indicating that TG65 femora were

less able than their wild type counterparts to sustain their structural integrity between the **time** of maximum load, when there are micro-cracks in the bone matrix, and the time of **failure** load, when the bone is broken, a feature of the ductility of the bone. This is **consistent** with the higher amount of disorganized matrix and higher matrix **mineralization** in these mice. D90 TG65 female biomechanical parameters were **alternatively** presented as histogram plots (Figure 16) illustrating that more transgenic **mice** are in the higher data range of failure moment, stiffness, moment of inertia, yet in **the** lower data range of energy to failure and post-yield deformation than wild type mice. **Taken** together, data suggest that TG65 femora have bigger bone geometry, yet may have **weaker** tissue-level material mechanical properties. .

Supporting data from FN70-TG24, FN29-TG01 and TG10 are shown in Table 8 and Table **9**. EI/I was 54.9% lower in female FN29-TG01 ($p=0.074$), 52.9% lower in female FN29-**TG** 10 ($p=0.076$) (Table 8); 48.8% lower in male FN29-TG 01 ($p=0.11$), and 52.9% lower **in** male FN29-TG 10 ($p=0.05$) (Table 10), while a similar trend was also observed in the **FN70-TG65**. No significant differences in failure moment and maximum moment, energy **to** failure and post-yield deformation were observed in FN29-TG01 and FN29-TG10. Since **FN29** bones have significantly bigger cross-sectional size (moment of inertia) and no **significant** difference in whole bone structural strength, FN29 bones may have weaker **material** properties as proposed above for FN70-TG65. However, FN29 did not show **changes** in ductility, as FN70-TG65 did. Energy to failure was decreased 23.4% ($p=0.038$) **in** female FN70-TG24 femora than those of the wild type, which was also consistent with **the** trend observed in FN70-TG65. Post-yield deformation was 32.8% lower in female

FN70-TG24, yet not statistically significant. These suggested a similar trend in changes in **bone ductility** in FN70-TG24 as in FN70-TG65. Interestingly, FN70-TG24 did not **demonstrate** changes in cross-sectional moment of inertia and EI/I in the same direction as **FN70-TG65**.

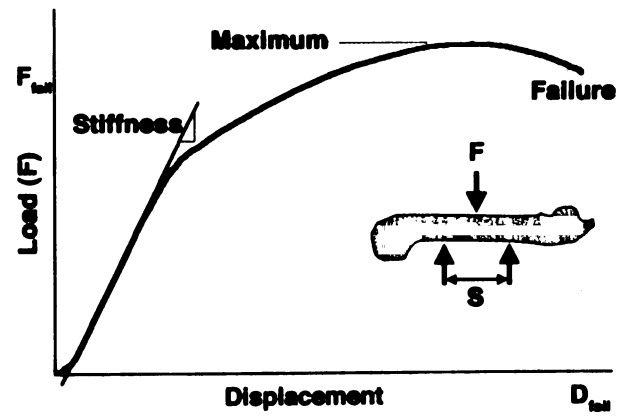


Figure 15. Schematic presentation of Load-Displacement curve for a bone specimen loaded in a three-point bending test and the associated mechanical properties that may be obtained from it. Skeletal functional integrity can be assessed by structural strength tests that measure how well the whole bone can bear loads (bending or torsion). In the three-point bending test, load was applied to failure in a 7mm span of the mid-diaphysis of a femoral bone to determine the structure's stiffness and failure load (structural strength). In a typical load-displacement curve, the Y-axis (load) is force loaded. The X-axis (displacement) is deformation under tension. The slope of the initial, straight part of the curve (elastic phase) gives stiffness, also known as Young's modulus of elasticity. Stiffness is a measure of the resistance to deformation under the applied load. Structural strength is the load required to fail (fracture) the whole bone. Taken together, both tissue level material mechanical properties and geometric properties affect the whole bone stiffness and failure load. Energy to failure (toughness) is the area under the curve at the ultimate failure point, which defines the work required to break the bone. When load is not proportional to displacement (yield), the elastic phase ends and the plastic phase starts and bone will no longer return to its original shape when the load is removed. The amount of post-yield displacement before ultimate failure defines material's ductility, which is an indicator of the material's ability to resist propagation of cracks. A material that manages little post-yield behavior before ultimate failure is considered brittle.

Table 8.1. FN70-TG65 femoral cortical bone tissue modulus is decreased and bone is less ductile in D90 female mice by three point bending test (Mean±SD)

genotype	N	Body WT	Failure Moment	Maximum Moment	Energy to Failure	Stiffness (EI)	EI/I tissue modulus	Moment of Inertia (I) (size)	Postyield Deformation
WT	8	24.2±1.4	24.3±2.6	33.1±1.6	8.3±0.9	167.7±37.4	1186±630	0.16±0.06	0.30±0.09
TG65F	9	24.0±1.2	31.3±5.9	36.6±4.0	6.6±1.5	281.1±98.9	877±352	0.34±0.07	0.12±0.09
Δ%		-0.8	+28.8	+10.6	-20.5	+67.6	-26.0	+112.5	-60.0
p-Value		0.8686	0.0028	0.0178	0.0392	0.0010	0.3747	0.0007	0.0048

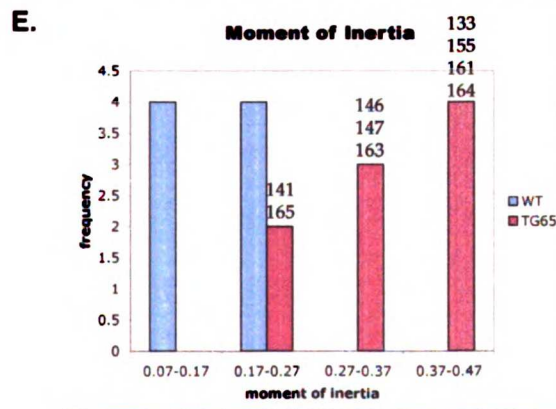
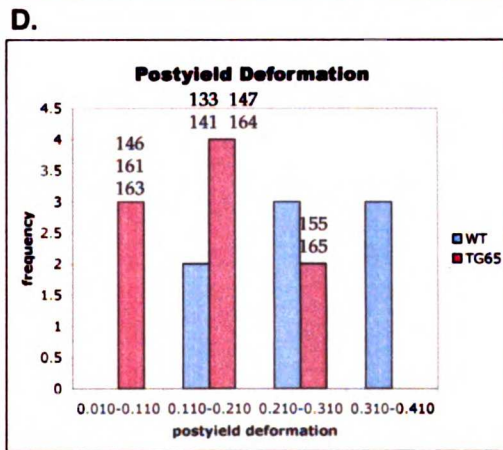
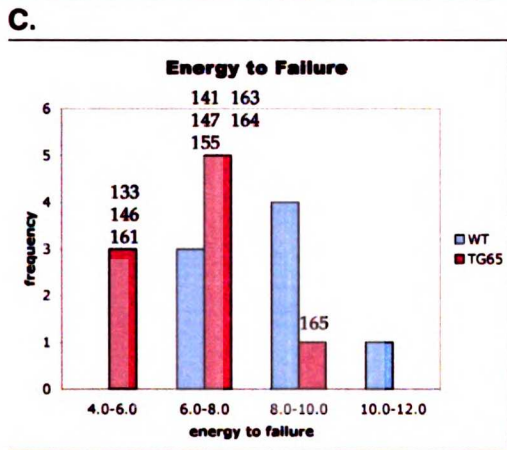
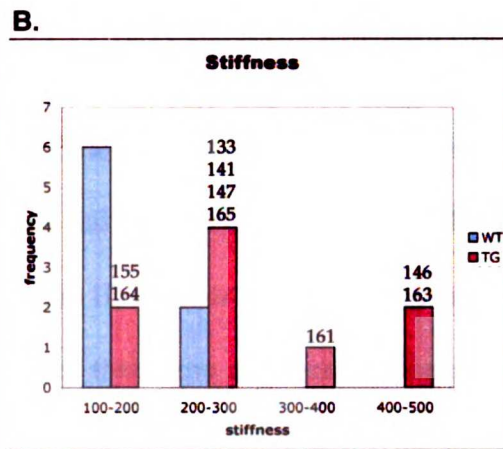
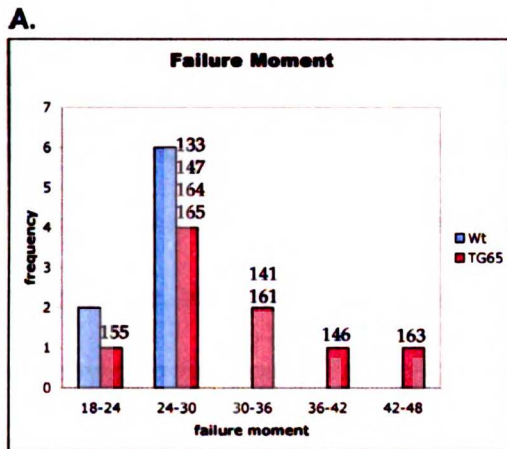


Figure 16. Histogram plot of mechanical strength measurements of femoral bones from 90-day old mice. The X-axis shows ranges of data for Failure Moment (A), Stiffness (B), Energy to Failure (C), Post-yield Deformation (D) and Moment of Inertia (E). The Y-axis shows the number of mice that fall into each data range. In the graph, wild type is blue, transgenic is red, and the unique ID number of each transgenic mouse is also shown on the graph. This graph illustrates that more transgenic mice are in the higher data range of bone failure moment, stiffness, and moment of inertia, but in the lower data range of energy to failure and post-yield deformation than wild type mice.

Table 9.1. Mechanical properties of cortical bone in the femurs from D90 FN29-TG01 (n=8) female mice by three point bending test (Mean±SD)

genotype	N	Body WT	Failure Moment	Energy to Failure	Stiffness (EI)	EI/I tissue modulus	Moment of Inertia (I)	Post-yield Deformation
TG01	8	24.8±1.5	26.2±5.2	8.1±2.3	174.7±55.0	535±153	0.34±0.09	0.25±0.14
Δ%		+2.5	+7.8	-2.4	+4.2	-54.9	+106.1	-14.0
p-Value		0.5497	0.5398	0.7925	0.8301	0.0738	0.0011	0.4783

Table 10.2. Mechanical properties of cortical bone in the femurs from D90 FN29-TG10(n=7) male mice by three point bending test (Mean±SD)

genotype	N	Body WT	Failure Moment	Energy to Failure	Stiffness (EI)	EI/I	Moment of Inertia (I)	Postyield Deformation
TG10	7	27.5±1.1	24.4±3.9	7.4±1.8	174.2±52.5	528±214	0.35±0.08	0.23±0.12
Δ%		-5.8	-2.5	+7.2	-7.5	-52.9	+59.1	+15
t-test		0.1572	0.7468	0.6508	0.6521	0.0586	0.0137	0.5512

Table 9.3. Mechanical properties of cortical bone in the femurs from D90 FN70-TG24(n=6) female mice by three point bending test (Mean±SD)

genotype	N	Body WT	Failure Moment	Energy to Failure	Stiffness (EI)	EI/tissue modulus	Moment of Inertia (I)	Post-yield Deformation
TG24F	6	22.7±0.2	25.1±4.5	6.4±1.3	199.9±56.2	2142±1512	0.14±0.11	0.20±0.12
Δ%		-6.2	+3.3	-23.4	+19.2	+80.6	-12.5	-32.8
p-Value		0.2161	0.3064	0.0383	0.3673	0.0171	0.6049	0.1357

Table 10.3. Mechanical properties of cortical bone in the femurs from D90 FN70-TG24(n=8) male mice by three point bending test (Mean±SD)

genotype	N	Body WT	Failure Moment	Energy to Failure	Stiffness (EI)	EI/I	Moment of Inertia (I)	Postyield Deformation
TG24	8	27.8±0.9	23.9±3.4	5.8±2.2	196.9±67.0	1317±814	0.17±0.05	0.18±0.08
Δ%		-4.8	-4.4	-15.9	+4.6	+17.4	-22.7	-10
t-test		0.2536	0.5454	0.2973	0.7794	0.5112	0.4187	0.5909

FN70-TG65 cortical bone is weaker in local material mechanical properties

To determine the micromechanical properties of the cortical bone tissue, a combined atomic force microscopy and nanoindentation technique was applied to measure the elastic modulus (E) and hardness (H) of the humeral cortical bone of the D90 FN70-TG65 transgenic and wild type female mice (in collaboration with Dr. Mehdi Blooch at UCSF). The mean and SD of elastic modulus and hardness were obtained by indentation on two different locations of the cortical bone each covering an area of $15\mu\text{m} \times 15\mu\text{m}$ (Figure 17). The elastic modulus of the wild-type bones is $20.9 \pm 1.3\text{GPa}$ and that of the FN70-TG65 bones is $16.6 \pm 0.9\text{GPa}$. The elastic modulus of the transgenic bones was significantly lower than that of the wild-type bones ($p=0.0014$). The hardness of the wild-type bones is $0.7 \pm 0.1\text{GPa}$ and that of the transgenic bones is $0.6 \pm 0.1\text{GPa}$. The hardness of the transgenic bones was significantly lower than that of the wild-type bones ($p=0.0218$).

Dynamic stiffness-mapping with simultaneous surface topography imaging also showed significantly lower elastic modulus of the transgenic bones in comparison to that of the wild-type bones (Figure 18). Elastic modulus data obtained this way was comparable with nanoindentation data, with wild-type at 23.7 ± 2.6 and transgenic at 16.2 ± 3.3 . Thus, local cortical bone material mechanical properties of 70kD FN transgenic mice are weaker. This is consistent with the decrease in EI/I and post-yield deformation described above in the whole bone three-point bending test.

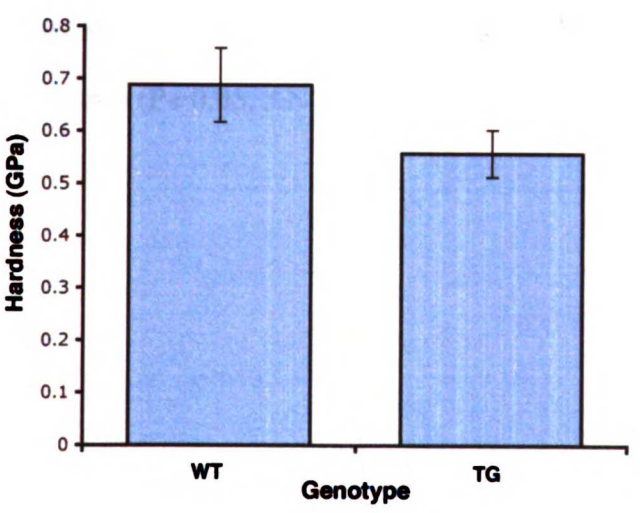
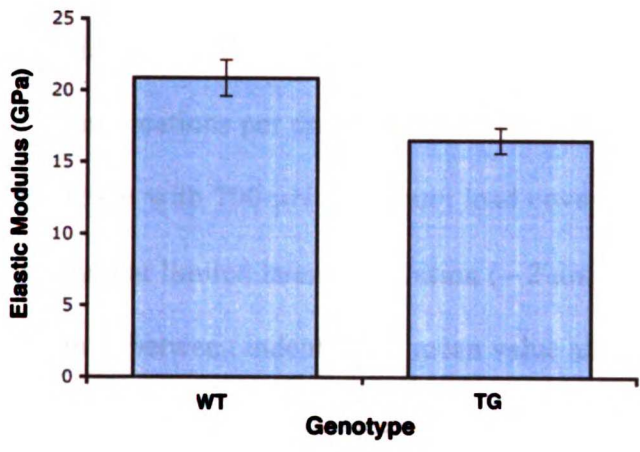


Figure 17. The elastic modulus (E) and hardness (H) of transgenic bones are significantly lower than those of the wild-type bones. The E and H of the bone material were obtained by a modified AFM and nanoindentation technique. Four each of the wild type and transgenic humeri were tested. Indentations were performed on two different locations per sample on the cortex in longitudinal sections of the bone. Indents were made with 700 μN maximum load covering a typical $15 \mu\text{m}^2$ area. This technique has inherent limited lateral resolution ($\sim 2 \mu\text{m}$), thus indents were made with an interval of $2\mu\text{m}$ in between indents. The mean value and standard deviation of elastic moduli and hardness of four different samples each for transgenic and wild type bones were shown on the graph. Data suggest that transgenic bones are much lower in E and H than wild-type bones ($P < 0.05$, ANOVA test).

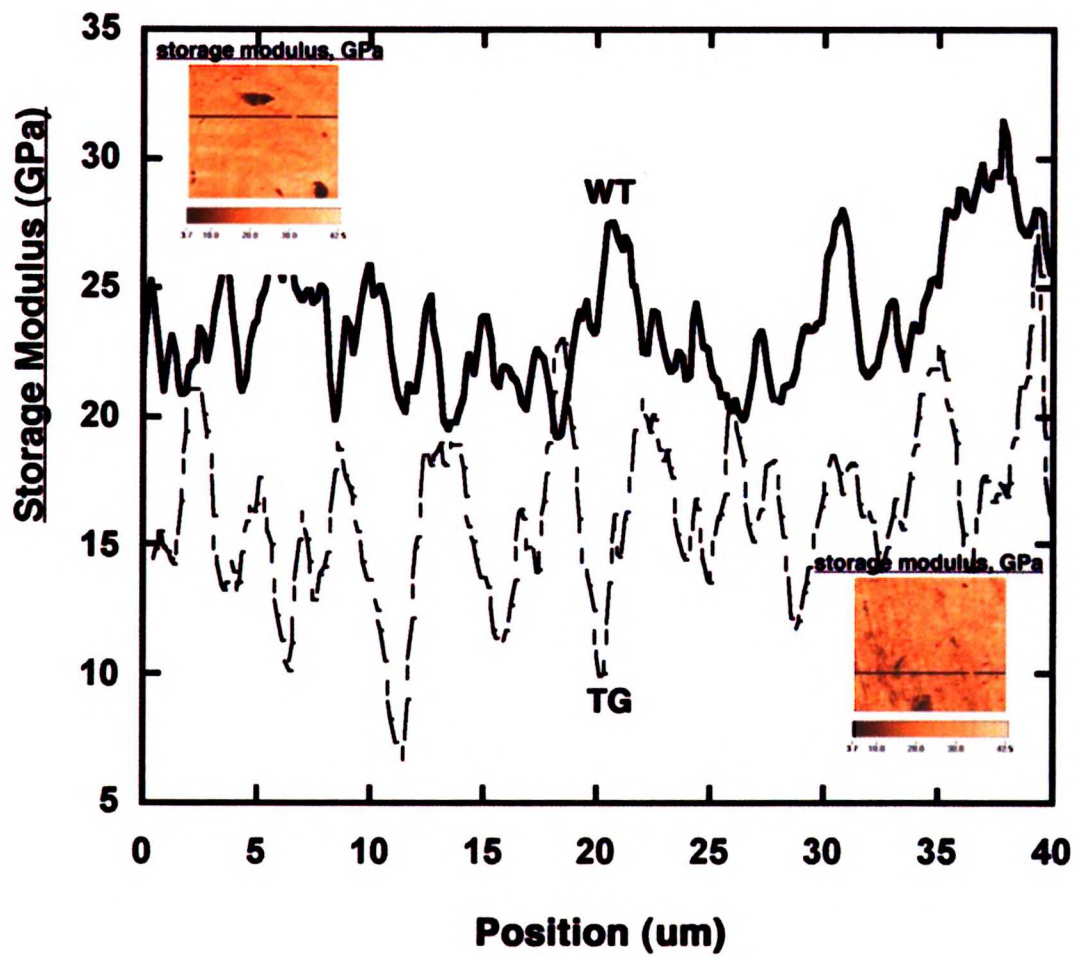


Figure 18. Elastic modulus mapping confirms the lower elastic modulus in transgenic bones in comparison to wild-type bones. Further modification of the AFM and nanoindentation technology allowed “dynamic stiffness” mapping (DSM) to obtain viscoelastic modulus images with indentation in the elastic phase of the tested material. This technique provides 65836 elastic modulus pixel readings and a lateral resolution of up to 20 nm in a single image. The calculated storage modulus is essentially equal to the elastic modulus for hard tissues such as bone. The quantitative storage modulus values along the black lines drawn on the images are plotted as a solid line (WT) and a dotted line (TG) for comparison. Significant reduction in storage modulus (elastic modulus) is apparent on transgenic bones compared to wild-type bones.

Summary of transgene phenotype

In summary, compared to wild type cortical bones, transgenic cortical bones show higher fraction of immature woven bone, increased endocortical bone formation rate, compromised bone material properties, reduced bone tissue modulus and ductility, small yet significantly increased bone mass and bone mineral density accompanied by either increased or no change in whole bone strength. Taken together, our results demonstrate that over-expression of 29kD or 70kD FN fragment in the bone affect bone homeostasis and result in changes in matrix organization, bone mass and bone quality.

A dramatic bone phenotype in 29kD FN transgenic line 08 (TG08) is unlikely relevant to transgene expression.

The 29kD FN line 08 mice were born viable, but some exhibited skeletal defects of both the calvarium and appendicular skeletons. Phenotype of the transgenic mice ranged from grossly normal to severely affected (Figure 19). Some transgenic mice did not show gross difference in size and appearance. A portion of the transgenic mice appeared smaller and showed exencephaly on the back of the head. Growth of these mice was severely delayed. Observation was made till one month of age when these mice were in clear stress and were sacrificed due to abnormal neurological disorders. Those with normal appearance may or may not contain small holes on the frontal bones of the calvarium (data not shown). Those with abnormal appearance invariably showed a larger than normal, midline foramen spanning the frontal bones, and the interparietal bones were smaller. X-ray radiographic analysis showed discontinuity of the vault of the calvarium and reduced bone mineral density of the long bones.

Microscopic examination of sagittal sections of the skull of transgenic mice at 2 weeks old revealed thinner parietal bones, presumably the consequence of retarded ossification. Transgenic mice showed decreased cancellous bone and cortical bone thickness (figure 20). TRAP staining of the whole calvaria in transgenic mice revealed localized accumulation of TRAP positive osteoclasts in comparison with evenly distributed single TRAP positive osteoclasts on the parietal bone of wild type mice. Taken together, some

line 08 transgenic mice demonstrated defect in both intramembranous and endochondrial bone formation.

Immunofluorescence staining of the calvaria sections with the fibronectin antibody showed distinctive network pattern of fibronectin staining resembling canalicular structure of the osteocytes. This network of fibronectin staining was largely lost in the calvaria section of the transgenic mice. Cause and effect relationship of fibronectin pattern with the bone phenotype was not clear with this study (Figure 21).

It was a puzzle why some transgenic mice exhibited no obvious bone phenotype while others with severely affected bone growth. Southern blotting with several different enzymatic digestion of genomic DNA was done with this line, which showed only one insertion site of transgene insertion (data not shown). Quantitative RT-PCR analysis also did not show difference in the level of transgene RNA expression. Taken together, the puzzle cannot be explained by alternative insertion site or RNA expression level. In addition, after several generations of inbreeding of transgenic mice line 08, some mice with negative transgene by PCR genotyping, that did not show transgene expression (presumably wild type) also exhibited similar bone phenotype. Overall, the bone phenotype described with 29kD FN transgenic line 08 may not be relevant to transgene expression of the 29kD fibronectin region in bone.

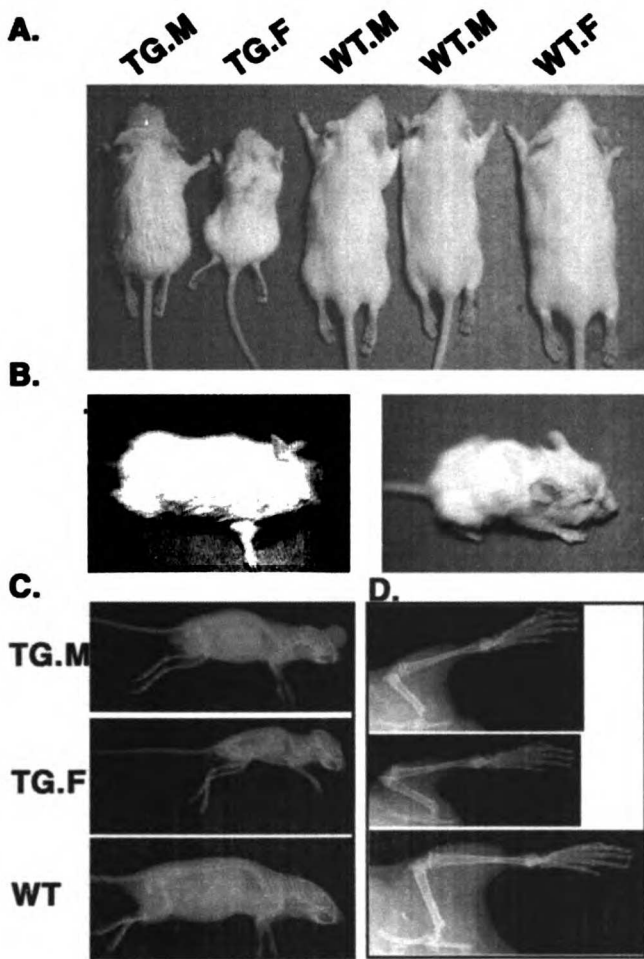


Figure 19. Gross appearance and abnormal development in calvaria and long bone in 35 day old 29kD FN transgenic mouse line 08 (FN29TG08). A. Initial litters of FN29TG08 mice were frequently smaller and developmentally delayed compared to their wild type littermates. B. Exencephaly was evident in 30% of the transgenic mice. C. Transgenic mice showed reduced integrity of bones forming the roof of the skull. D. Transgenic femurs and tibias were shorter and showed decreased cancellous bone density.

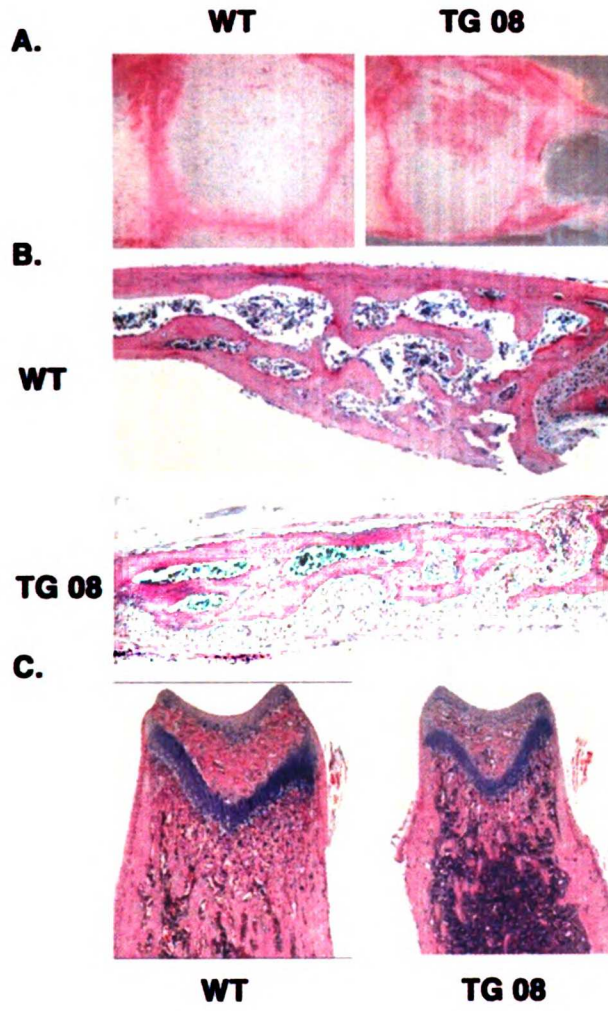


Figure 20. Histological appearance of transgenic calvaria and femur at 35 day old.

A. Whole mount calvarial TRAP staining of osteoclasts. TRAP positive osteoclasts were evenly distributed on the endosteal surface in wild type mice; while clustered on the parietal bone endosteal surface in the transgenic mice. Also shown is a large hole in the frontal bone of a transgenic calvaria. B. H & E staining of saggital sections of wild type and transgenic calvaria. Transgenic calvaria appeared developmentally delayed especially at the suture and on the endosteal surface, showing a significant amount of connective tissue. C. H & E staining of a longitudinal section of femurs of wild type and transgenic mice. Transgenic mice showed significantly decreased cancellous bone and reduced cortical bone thickness .

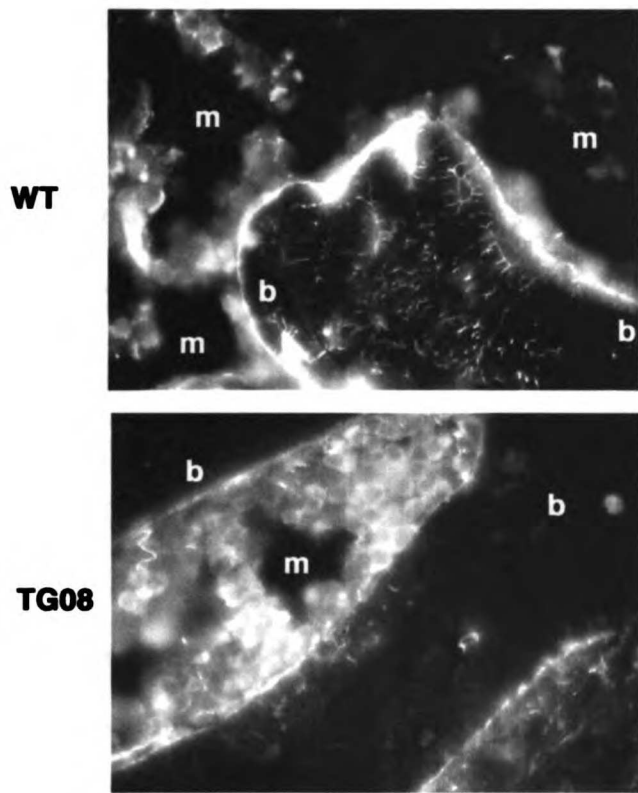


Figure 21. Immunofluorescence staining of calvarial bone sections at 35 day old using rabbit polyclonal anti-fibronectin antibody. On wild type bone sections, fibronectin staining the bony areas revealed an extensive network pattern, while staining on the transgenic bone section was scarce. Abbreviations: b, bone; m, bone marrow.

DISCUSSION

The primary process of bone formation is the deposition, organization and mineralization of bone extracellular matrix (ECM). One of the major non-collagenous ECM components in bone is fibronectin (FN). FN regulates the deposition, organization and stability of other ECM molecules such as type I collagen and thrombosponin-1 (McDonald *et al.*, 1982; Sottile *et al.*, 2002), tenascin C (Chung and Erickson, 1997) and fibulin (Roman and McDonald, 1993; Godyna *et al.*, 1995; Sasaki *et al.*, 1996) *in vitro*. FN is deposited at high levels in skeletal tissue and its expression is highly regulated in specific stages of osteoblast differentiation *in vitro* (Stein *et al.*, 1990; Winnard *et al.*, 1995; Vary *et al.*, 2000) and skeletogenesis *in vivo* (Kosher *et al.*, 1989; Moursi *et al.*, 1996 and 1997). FN plays essential roles in osteoblast differentiation and survival *in vitro* (Moursi *et al.*, 1996 and 1997; Globus *et al.*, 1998). ECM interaction with cell surface receptors (e.g. integrins) can transduce signals from outside to inside the cell and this interaction is crucial for the formation and homeostasis of all tissues (Damsky, 1997). The $\beta 1$ family of integrins is expressed strongly in bone (Moursi *et al.*, 1997). The integrin $\beta 1$ subunit forms heterodimers with many α subunits. Several of these heterodimers can recognize FN. $\beta 1$ integrins have been shown to play critical roles *in vivo* in bone and several other tissues to regulate matrix deposition and organization and tissue formation (Sasaki, 1998, Faraldo, 1998, and Zimmerman, 2000). To understand directly the function of FN in bone formation and bone remodeling *in vivo*, we generated transgenic mice that express either the 29kD or 70kD fragments of the N-terminal matrix assembly domain of FN in mature osteoblasts and osteocytes. The rationale for using these fragments was to perturb

endogenous FN fibrillar matrix assembly, thus serving as a dominant inhibitor of FN function *in vivo* in the bone. In this study, we have characterized two independent transgenic lines each of the 29kD (FN29-TG01 and FN29-TG10) and 70kD FN (FN70-TG24 and FN70-TG65) expressing transgenic mice with the greatest in-depth focus on FN70-TG65 due to its relatively high level of detectable transgene protein expression. The significant observations in transgenic mice compared to wild type mice are: more disorganized immature cortical bone, compromised bone material properties, increased bone mass and bone mineral density accompanied by either an increase or no change in whole bone strength. Based on our results, we propose that overexpression of 29kD and 70kD FN affects osteoblast function and bone matrix formation *in vivo* by several mechanisms.

FN fragments regulate bone remodeling and/or bone matrix organization

The primary phenotype of TG mice was an increase in cortical woven bone. The presence of increased woven bone in TG suggests either a higher rate of new bone formation or delayed or defective remodeling of woven bone matrix into lamellar bone matrix. The increase in TG cortical bone thickness, volume and density provides a clue that TG has a higher net gain in bone formation relative to bone resorption in comparison with WT. However, whether the net gain is due to relatively higher bone formation or lower bone resorption is unclear using this approach alone. Direct evidence for the rate of new bone formation can be provided by dynamic histomorphometry analysis of bone sections of mice injected sequentially with two fluorochrome labels which incorporate into newly

formed bone matrix at sites of mineralization (Villanueva, 1983). Preliminary histomorphometric analysis suggests that TG has two fold higher endocortical bone formation. Higher fraction of woven bone along with increased endocortical bone formation have also been reported in mice treated locally or systemically with anabolic agents such as prostaglandin E₂ (PGE₂), PTH and in transgenic mice with systemic or bone-specific over-secretion of growth hormone (GH) and bone-specific overexpression of soluble colony-stimulating factor-1 (sCSF-1). Interestingly, signals from ECM can synergize with signals from growth factors to regulate a wide range of cellular functions such as gene expression, differentiation and survival (Damsky and Werb, 1992; Miyamoto, 1996; Giancotti 2000; Sieg et al., 2000). PTH has been shown to increase FN production in cultured bone cells and fetal bones *in vitro* and increase circulating levels of FN *in vivo* (Eielson, 1994 and Sun, 1997). Thus, the similarity of this aspect of the FN TG bone phenotype with the above mentioned soluble anabolic factors suggest a possible functional linkage of these two pathways in the bone. Besides accelerated new bone matrix deposition, delayed or defective remodeling of woven into lamellar bone matrix may also contribute to the increased woven bone phenotype in transgenic mice. This remodeling process encompasses both the resorption of the randomly oriented collagen matrix and the replacement with the parallel lamellar collagen matrix. Expression of dominant-negative integrin receptor $\beta 1$ chimera in mature osteoblasts and osteocytes leads to a similar increase in woven bone fraction attributable to defect in the formation and organization of bone matrix (Zimmerman, 2000). This hypothesis of a direct role of FN in woven bone remodeling and lamellar bone organization are consistent with *in vitro* and *in vivo* function of FN in tissue organization, matrix composition and remodeling in a

number of different systems. FN is essential for organization of heart and blood vessels and assembly of endothelial basement membrane, and thus FN null mutation in mouse embryos results in lethal cardiovascular defects (George et al., 1997; Francis et al., 2002). FN fragments in cartilage with 29kD FN the most potent one lead to severe cartilage damage or couple repair to damage in a dose dependent manner in an *in vitro* as well as an *in vivo* model of cartilage damage (Homandberg, 1999). High concentrations of 29kD FN fragments upregulate expression of matrix metalloprotease (MMP), stimulate release of catabolic cytokines, enhance degradation and loss of proteoglycan (PG) from cartilage and suppress PG synthesis as observed in osteoarthritis. Low concentrations of 29kD FN fragments elicit release of anabolic cytokines and stimulate PG synthesis to limit cartilage damage. Therefore, FN fragments appear to regulate cartilage matrix composition and remodeling in a dose dependent manner. FN fragments have also been reported in other pathological body fluids (e.g. wound fluid) and tissues and may also play important roles in coupling repair to damage (Carsons, 1987; Easter et al., 1988; Skrha et al., 1988 and 1990; Wysocki and Ginnell, 1990; LaCelle et al., 1991; Allal et al., 1992 and Suzuki et al., 1992). FN deposition *in vivo* represents the initial event during fibrillogenesis of connective tissue matrices occurring during embryogenesis and wound healing (McDonald, 1988; Colvin, 1989; Thiery et al., 1989). FN can bind to collagens through several collagen binding sites (Colombi, 2003), and FN binding sites in collagen molecules have been reported (Dzamba et al., 1993 and Ingham, 2002). Many data indicate the interdependence of FN and collagen network assembly; in particular, in several cell systems, the assembly of collagens has been shown to depend on FN organization (McDonald, 1988; Velling et al., 2002 and Sottile et al., 2002), whereas, in

others, collagens have been shown to influence FN fibrillogenesis (Dzamba, 1993; Chernousov et al., 1998 and Zoppi et al., 2004). In this study, we show that overexpression of FN fragments in bone leads to more poorly organized bone matrix as reflected by both collagen fibers and osteocytes oriented in different directions. Therefore, we propose that FN fragments may directly interfere with organization of FN and collagen fibrillar matrix and further bone microstructural organization (e.g. Lamellae, osteons). Though there is yet no solid experimental data suggesting the functional linkage between FN and collagen in bone matrix organization *in vivo*, direct evidence for FN as a key regulator of assembly of bone ECM proteins has recently been presented using an *in vitro* osteoblast culture model derived from FN null embryonic fibroblasts (ASBMR abstract 2004). In this system, FN null embryonic fibroblasts can differentiate into mature osteoblasts, yet ECM assembly is impaired and mineralization fails to occur. Reconstitution in the culture by addition of exogenous FN during the entire culture period rescued the ECM assembly and mineralization. Intriguingly, exogenous FN has to be supplied continuously to maintain FN fibrillar matrix and other ECM stability.

Taken together, the mechanism of remodeling of woven bone matrix to organized lamellar structure remains poorly understood. Interpretation of the mechanistic relationship of FN fragments and observed bone phenotype of increased woven bone fraction is further complicated by the difficulty of following the dynamic process of matrix organization in bone *in vivo* and the fact that FN fragments could have cryptic function not shared by intact FN such as their role in MMP induction. Bone-specific conditional knockout of FN using cre-recombinase driven by osteocalcin promoter will

likely shed more lights on the *in vivo* function of FN in bone ECM organization, maturation and mineralization.

FN fragments regulate cortical bone mass

The higher woven bone fraction observed in FN70 TG mice was accompanied by an increase in cortical bone mass (BV/TV), cortex thickness and mid-diaphyseal cross-sectional size. This increase in bone mass was apparent by postnatal D35 with significant increase in bone mass (7.9%), cortex thickness (12%), cortex volume (18%), and no difference in marrow volume. At postnatal D90, TG has significant increase in bone mass (7.6%), cortex thickness (8%), cortex volume (6%) and a prominent decrease in marrow volume (12%). Several features of this phenotype are worthy of attention. First, the percentage difference in bone mass between WT and TG is evident by D35 and remain similar at D90. Thus, the net gain in bone mass from D35 to D90 in TG mice was not significantly different from WT suggesting that TG effect on cortical bone mass was mainly developed during pre-pubertal period of rapid bone growth, the so-called bone modeling period. Second, TG (female) shows no significant difference in body weight and bone length at D35, thus, the FN TG exerts an anabolic effect on bone appositional growth rather than longitudinal growth. Third, D35 TG demonstrates increase in cortex volume and thickness yet similar marrow volume indicating a positive effect on periosteal bone apposition during rapid bone growth. Lastly, D90 TG shows significant marrow narrowing in comparison to D35TG and D90 WT indicating an increase in endocortical bone formation between D35 and D90. Taken together, FN TG appears to serve as an anabolic signal for bone matrix apposition at the periosteal surface pre-pubertally and the endosteal

surface post-pubertally. Cellular mechanisms underlying this phenotype await histomorphometric analysis of the bone formation rate and the quantification of the number of osteoblasts, osteocytes and osteoclasts. Nevertheless, bone mass in mature animals is maintained by a delicate balance between matrix-forming osteoblasts and matrix-degrading osteoclasts, a process named bone remodeling. Bone remodeling in response to mechanical stimuli enables bones to adapt their material structures and bone mass to meet mechanical demands as often referred to as “Wolff’s Law”. Therefore, the mechanisms with which the TG mice attain higher initial bone mass and subsequently reorient the location of remodeling can be two fold, a direct transgene effect on bone modeling or remodeling with net increase in bone formation or indirect skeletal adaptation to mechanical stimuli to compensate for material deficit or both. The D90 phenotype is attributable at least partially to the increased endocortical bone formation as demonstrated by preliminary histomorphometric analysis of D90 TG cortical bones. However, the possibility of geometric adaptation in response to poor matrix quality cannot be excluded. Intriguingly, Osteogenesis imperfecta (OI), an autosomal dominant genetic disease caused by mutations in type I collagen genes, is also characterized by defective bone matrix and impaired matrix mechanical properties. Several mouse models of OI have demonstrated adaptations to compensate for the compromised matrix mechanical quality by increasing cortical bone cross-sectional geometry (Bonadio, 1993, Pereira 1995, McBride, 1998). Thus, the higher fraction of defective bone matrix and impaired matrix mechanical quality in the FN TG may elicit similar geometrical compensatory mechanism to maintain optimal bone strength. However, we have yet no evidence for the cause of this anabolic response. Similar anabolic effect on matrix deposition has also been reported in *in vitro* and *in vivo* cartilage

damage/repair model by FN fragments. High concentrations of FN fragments enhance release of catabolic cytokines and reduce cartilage PG content leading to cartilage damage, while low concentrations of FN fragments enhance PG synthesis and PG content triggering repair response to limit damage. One possible model was proposed and tested in the cartilage. Low concentrations of FN fragments enhance release of anabolic growth factors including TGF β and IGF-1. As low concentration also upregulate MMPs, limited proteolysis could be involved in activation of these growth factors which are otherwise inactive when trapped in the matrix. Consistent with this model, overexpression of IGF-1 in mature osteoblasts and osteocytes, using the osteocalcin promoter, increases bone formation rate and trabecular bone density and volume (Zhao et al., 2000). Therefore, FN70 TG may enhance bone matrix deposition by modulating the activation state of the inert IGF trapped in bone matrix. Intriguingly ternary complex of IGF-1/IGFBP-3/FN is detected in human plasma and FN is suggested to play a role in the transportation of these proteins in the circulation and sequestration of them in the tissue (Gui and Murphy, 2001). On the other hand, ECM-integrin signaling is also known to regulate cellular proliferation, differentiation and function by synergizing with the activation of growth factors in a number of cell systems including osteoblasts. Osteoblasts and their progenitors fail to respond to IGF-1 when bones are relieved of the burden of bearing weight. And the resistance to IGF-I induced by skeletal unloading can be attributed to a reduction in the integrin/IGF-I receptor interaction (Takeshi et al., 2004). Functional perturbation of collagen-integrin interaction blocked the differentiation of osteoblast progenitor cells induced by BMP2, a member of the TGF β /BMP superfamily (Jikko et al., 1999). Conversely, BMP can enhance FN synthesis and FN fibrillogenesis in vitro primary rat

osteoblasts (Tang et al., 2003). Therefore, FN fragments may also regulate bone mass by modulating signals from the growth factors.

FN fragments regulate biomechanical properties of the bone

Cortical bone contributes significantly to the mechanical strength of an individual bone (Spadaro et al., 1994; Augat et al., 1998 and Bell et al., 1999). Skeletal functional integrity as assessed by structural strength test is dependent on both the bone material properties and the bone geometry. Because the increased woven bone and weak material properties in FN70-TG65 cortex are accompanied by increased cortical bone mass and cross-sectional area, the whole bone strength (failure moment and stiffness) is either increased or normal in TG mice in comparison to WT mice. However, energy to failure (a measurement of the work that must be done per unit volume on the specimen before it breaks) and normalized stiffness by cross-sectional size (EI/I , tissue modulus of elasticity, an indication of how stiff the bone material is) are decreased. These suggest a deficiency of the quality of the bone material. Indeed, there is a decrease in the elastic modulus and hardness of the bone material as assessed in bone material property measurements by AFM. In addition, decreased post-yield deformation, a property of the bone after yield and before fracture, indicates a reduced ductility of the bone material. FN70-TG24 shows similar trend of decrease in energy to failure and post-yield deformation, but not the tissue modulus of elasticity suggesting that lower level of 70kD FN expression in TG24 affect negatively the bone material ductility, but not modulus of elasticity. Consistent with the mechanical adaptation model proposed above, there is no increase in cross-sectional size in this line either. In contrast, FN29-TG01 and FN70-TG10 exhibited reduction in tissue modulus of

elasticity and increase in cross-sectional size, yet no difference in energy to failure and post-yield deformation. Intriguingly, FN29 differ in lacking the 40kD collagen-binding domain present in the FN70. Plus, there is a 40kD band present in the Western blot of the FN70 bone lysate detected by HA epitope tag antibody, stressing that this 40kD band may as well be the *in vivo* degradation fragment of the collagen-binding domain of the 70kD FN. Therefore, it is likely that the 40kD collagen-binding domain is one of the major determinants in the phenotypic change in the bone material ductility in FN70-TG65 and FN70-TG24 while the 29kD matrix assembly domain may be the major contributor in the difference in elastic modulus of the bone material.

The mechanical properties of bone material are determined by the relative amounts and quality of its 3 major constituents: mineral, water, and organics (mainly type I collagen) as well as the organization of the resulting material at both the microscopic and macroscopic scales (Currey, 2003; Boskey et al., 1999; Meulen et al., 2001; Martin and Ishida, 1989; Currey, 1988; Burstein, 1975; and Martin and Boardman, 1993). FN TG mice have two characteristics which may contribute to the reduced quality and ductility of the bone material: 1) an increase in the ratio of woven to lamellar bone reflecting a higher percentage of area of bone with deranged collagen deposition and 2) an increase in bone mineral density. On the other hand, compromised local material properties at the bone tissue level further support the notion that TG bone is defective in the composition and/or organization of matrix and/or mineral.

Extensive literature has demonstrated the existence of a mechanistic link between reduced quantity of collagen and other extracellular matrix and abnormal collagen fibrillar structure and organization with diminished bone mechanical properties (Masse et al., 1996; Spendgler et al., 1977; Mehta and Antich, 1998; Camacho et al., 1999; Riggs et al., 1993; Martin et al., 1996 and Boskey et al., 1999). In particular, collagen fiber orientation was highly correlated with mechanical properties in the cortical bone of the equine radius (Riggs et al., 1993). In addition, the observation of collagen deposition parallel to lines of mechanical stress suggests that collagen organization may contribute to the ultimate biomechanical performance of bone. Indeed, animal studies support this proposal and find that longitudinally oriented collagen is correlated with greater modulus and strength, and remodeling was associated with more transverse collagen (Martin et al., 1996). The higher organization of collagen due to the adaptation of the bone organic matrix to mechanical stimulus may be contributing to the maintenance of the ultimate biomechanical strength of the bone (Puustjarvi et al., 1999). In our study, FN TG expression in bone leads to increased percentage of woven bone characterized by more transverse and less-well-aligned collagen fibrils resulting in the weak bone phenotype. However, the effect may be partially indirect since deranged collagen itself leads to variable mineral crystal size and orientation (Grabner et al., 2001). Therefore, It is difficult to separate mechanical effects of collagen and mineral in this model. In addition, FN matrix assembly increases the ultimate strength and toughness of collagen biogels *in vitro* suggesting FN's direct role in enhancing the mechanical performance of the bone tissue (Gildner, 2004). Yet, this is unlikely to be the major contributor in the phenotype of weak bone material properties since FN is a minor component in the final bone matrix.

In addition to the effect of the amount and quality of collagen on bone material properties, changes in mineral are also considered as contributing factors in the diminished mechanical properties. However, there remains the question why the bone shows a greater degree of mineralization. Similarly, a greater degree of mineralization has also been reported in the bone of the murine model (oim/oim) of osteogenesis imperfecta (OI) and some cases of human OI with a genetic mutation in type I collagen resulting in altered collagen molecular structure (Grabner et al., 2001; Bovde et al., 1999 and Jones et al., 1999). This has been linked in both cases to the brittleness of these tissues. Increased mineralization may be a common response for bone tissues with inherent weakness attributable to defective collagen. The advantage of such attempt to stabilize bone tissue by increasing bone mineral density is offset by the increased brittleness. On the other hand, bone mineral density and mechanical strength generally show positive correlations (Burstein et al., 1975 and Currey, 1969). In our study, it seems initially contradictory that there is both increased mineralization and decreased modulus elasticity and hardness of the bone material. Yet, this dissociation of mineral density and material properties is not so unusual. Osteopetrosis, a group of metabolic bone diseases, presents with both increased skeletal density and increased risk of fracture. Osteopetrotic mutations in the rat lead to weaker bones in spite of greater mineral density and bone mass (Tuukkanen, 2000). Furthermore, bones from oim mice, a murine model of human OI, show weaker material properties even though the mineral content is normal or slightly higher (Camacho 1999). In both cases, there are evidences that mineral crystal size and shape and its distribution in relationship with collagen are irregular, indicating the importance of mineral quality in bone material

mechanical properties (Wojtowicz, 1997 and Camacho 1999). It is hypothesized that a defective collagen matrix in OI serves as an abnormal template for mineralization. Given the apparent disorganization of matrix in FN70-TG as well as OI, it is possible that the quality of the mineral is defective as illustrated in OI showing the presence of smaller than normal mineral crystals with altered mineral characteristics and the presence of mineral outside the collagen fibrils (Camacho et al., 1996; Vetter et al., 1991; Traub et al., 1994; Cassella et al., 1995 and 1996). Further studies in FN70 TG mice using X-ray diffraction, FTIR, and Ca:P analysis will shed more light on the mineral quality in these TG mice. Therefore, our FN70-TG model is another illustration that an increased bone mineral density does not necessarily lead to stronger bones.

In conclusion, worthy of attention is the phenotypic resemblance of the FN70 TG mice with the murine models of mild form of human OI such as heterozygous *Mov13* and *oim* mice: regional disorganized matrix in the cortical bone characterized by less intense staining, abnormal organization of bone cells and disorganized collagen using polarized light microscopy (Bonadio et al., 1990); increased cortical thickness due to altered endocortical or periosteal bone formation; and significantly reduced mechanical and material properties. This phenotypic similarity poses a possible functional linkage of FN and collagen both in aligning an oriented fibrillar matrix and in the structural and functional integrity of the bone.

Future directions

The primary phenotype of the 70kD FN transgenic mice was an increase in cortical bone mass accompanied by an increase in cortical immature woven bone at both D35 and D90. Dynamic histomorphometric analyses showed that increased endocortical osteoblastic bone formation was contributing to the higher cortical bone mass in D90 transgenic mice. The rate of osteoclastic bone resorption and the bone cell profiles *in vivo* remain to be established. However, the two-fold increase in bone formation rate and only 8% increase in cortical bone volume suggested that the rate of bone resorption is likely to be elevated as well. Further histomorphometric analyses shall be performed to demonstrate *in vivo* bone cellular profiles including the osteoblast number and surface, osteoclast number and surface, osteocyte density and osteocytic lacunae occupancy. This may provide new clues to the cellular mechanism of the bone phenotype.

The higher fractions of woven bone containing Haversian canals and the higher number of tunnel-like structures suggested similarity to Haversian remodeling. Several lines of experiments can further test this hypothesis: 1. Quantification of cortical porosity by histomorphometric analysis. 2. Localization of pores in the cortex by μ CT. 3. Histomorphometric analyses of osteoclast perimeter and erosion pits on the endocortical bone surface. 4. Visualization of fluorochrome labels along the perimeter of the intracortical pores. This may provide further mechanism for the lower cortical bone material properties in the transgenic mice.

The increased endocortical bone formation *in vivo* appeared to relate both to the increased bone surface undergoing formation and the increased matrix production. Therefore, it will be interesting to determine whether the altered osteoblast phenotype was due to transgene effect on osteoblast differentiation or function using primary osteoblasts derived from calvaria of the transgenic and wild type mice. The expression of osteoblast markers, assembly and organization of ECM and the ability to form mineralized nodules will be followed up during the time course of the differentiation of primary calvarial osteoblasts *in vitro*.

It is also interesting to note that the phenotype was predominantly in the cortical bone and the trabecular bone did not show differences in bone mass and bone formation rate. Transgenic mice expressing a dominant negative integrin $\beta 1$ driven by the same osteocalcin promoter also demonstrate a predominant cortical bone phenotype. Regional differences in osteocalcin promoter activity may not be the only explanation. Cortical bone contributes more significantly to the mechanical strength of an individual bone compared to trabecular bone. Thus, local regulation of osteoblastic bone formation in response to mechanical demands may differ in the cortical bone versus the trabecular bone. Furthermore, bone ECM and the ECM integrin receptors have been proposed as candidate molecules in mediating this mechano-signaling transduction pathway. To address whether transgene expression modulates the response of bone to different mechanical environment, stabilized and non-stabilized bone fracture repair models can be exploited to examine the rate and stages of fracture repair in transgenic mice compared to wild type mice. In addition, fibronectin provides a crucial substrate for many forms of cell adhesion and cell

migration. Thus, the process of osteoclast migration and vascular invasion can be traced during different time points of fracture healing. This may facilitate mechanistic understanding of the role of fibronectin transgene in bone formation in response to mechanical environment.

REFERENCES

Allal M, Robert L, Labat-Robert J 1992 Fragmentation of fibronectin in cystic fibrosis. *C R Acad Sci III* 314:587-592.

Augat P, Fan B, Lane NE, Lang TF, LeHir P, Lu Y, Uffmann M, Genant HK 1998 Assessment of bone mineral at appendicular sites in females with fractures of the proximal femur. *Bone* 22:395-402.

Bell KL, Loveridge N, Power J, Garrahan N, Stanton M, Lunt M, Meggitt BF, Reeve J 1999 Structure of the femoral neck in hip fracture: Cortical bone loss in the inferoanterior to superoposterior axis. *J Bone Miner Res* 14:111-119.

Bonadio J, Saunders TL, Tsai E, Goldstein SA, Morris-Wiman J, Brinkley L, Dolan DF, Altschuler RA, Hawkins JE, Bateman J F jr. 1990 Transgenic mouse model of the mild dominant form of osteogenesis imperfecta. *Proc Natl Acad Sci* 87: 7145-49.

Bonadio J, Jepsen KJ, Mansoura MK, Jaenisch R, Kuhn JL, Goldstein SA 1993 A murine skeletal adaptation that significantly increases cortical bone mechanical properties. Implications for human skeletal fragility. *J Clin Invest.* **92(4):**1697-705.

Boskey AL, Wright TM, Blank RD 1999 Collagen and bone strength. *J Bone Miner Res.* **14:** 330-335.

Boyde A, Travers R, Glorieux FH, Jones SJ 1999 The mineral density of iliac crest bone from children with osteogenesis imperfecta. *Calcif Tissue Int* **64:**185–190.

Burstein AH, Zika JM, Heiple KG, Klein L 1975 Contribution of collagen and mineral to the elastic-plastic properties of bone. *J Bone Joint Surg Am.* **57:**956-961.

Camacho NP, Landis WJ, Boskey AL 1996 Mineral changes in a mouse model of osteogenesis imperfecta detected by Fourier transform infrared microscopy. *Connect Tissue Res.* **35:**259-265.

Camacho NP, Hou L, Toledano TR, Ilg A, Brayton CF, Raggio CL, Root L, Boskey AL 1999 The material basis for reduced mechanical properties in *oim* mice bones. *J Bone Miner Res.* **14:**264-272.

Carsons S 1987 High levels of fibronectin fragments in the plasma of a patient with active systemic lupus erythematosus. *J Rheumatol* **14**:1052-1054.

Cassella JP, Garrington N, Stamp TC, Ali SY 1995 An electron probe X-ray microanalytical study of bone mineral in osteogenesis imperfecta.. *Calcif Tissue Int.* **56**:118-122.

Cassella JP, Stamp TC, Ali SY 1996 A morphological and ultrastructural study of bone in osteogenesis imperfecta.. *Calcif Tissue Int.* **58**:155-165.

Chernousov MA, Sthal RC, Carey DJ 1998 Schwann cells use a novel collagen dependent mechanism for fibronectin fibril assembly. *J. Cell Sci.* **111**:2763–2777.

Colombi M, Zoppi N, De Petro G, Marchina E, Gardella R, Taviani D, Ferraboli S, Barlati S 2003 Matrix assembly induction and cell migration and invasion inhibition by a 13-amino acid fibronectin peptide. *J. Biol. Chem.* **278**:14346–14355.

Colvin RB 1989 *Fibronectin* In: Mosher DF (ed.) *Fibronectin*. Academic Press Inc., San Diego, USA, pp. 213–254.

Currey JD 1969 The mechanical consequences of variation in the mineral content of bone. *J Biomech.* 2:1-11.

Currey JD 1988 The effect of porosity and mineral content on the Youngs modulus of elasticity of compact bone. *J Biomech.* 21:131-139.

Damsky CH, Werb Z 1992 Signal transduction by integrin receptors for extracellular matrix: cooperative processing of extracellular information. *Curr Opin Cell Biol.* 4:772-81.

Damsky CH, Moursi A, Zhou Y, Fisher SJ, Globus RK 1997 The solid state environment orchestrates embryonic development and tissue remodeling. *Kidney Int.* 1:1427-33.

Dzamba BJ, Wu H, Jaenish R, Peters DM 1993 Fibronectin binding site in type I collagen regulates fibronectin fibril formation *J. Cell Biol.* 121:1165–1172.

Easter DW, Hoyt DB, Ozkan AN 1988 Immunosuppression by a peptide from the gelatin binding domain of human fibronectin. *J Surg Res* 45:370-375.

Eielson C, Kaplan D, Mitnick MA, Paliwal I, Insogna K 1994 Estrogen modulates parathyroid hormone-induced fibronectin production in human and rat osteoblast-like cells. *Endocrinology* **135**:1639-44.

Faraldo MM, Deugnier MA, Lukashev M, Thiery JP, Glukhova MA 1998 Perturbation of beta1-integrin function alters the development of murine mammary gland. *EMBO J.* **17**: 2139-2147.

Filvaroff EH, Guillet S, Zlot C, Bao M, Ingle G, Steinmetz H, Hoeffel J, Bunting S, Ross J, Carano RA, Powell-Braxton L, Wagner GF, Eckert R, Gerritsen ME, French DM. 2002 Stanniocalcin 1 alters muscle and bone structure and function in transgenic mice. *Endocrinology* **143**:3681-90

Francis SE, Goh KL, Hodivala-Dilke K, Bader BL, Stark M, Davidson D, Hynes R 2002 Central roles of alpha5beta1 integrin and fibronectin in vascular development in mouse embryos and embryoid bodies. *Arteriosclerosis, Thrombosis and Vascular Biology* **22**:927-933.

George EL, Baldwin HS, Hynes RO 1997 Fibronectins are essential for heart and blood vessel morphogenesis but are dispensable for initial specification of precursor cells. *Blood* **90**:3073-3081.

Giancotti FG 2000 Complexity and specificity of integrin signalling. *Nat Cell Biol.* **2**:E13-4.

Gildner CD, Lerner AL, Hocking DC 2004 Fibronectin matrix polymerization increases tensile strength of model tissue. *Am J Physiol Heart Circ Physiol.* **287**(1):H46-53.

Globus RK, Doty SB, Lull JC, Holmuhamedov E, Humphries MJ, Damsky CH 1998 Fibronectin is a survival factor for differentiated osteoblasts. *J Cell Sci.* **111**:1385-93.

Globus RK, Amblard D, Nishimura Y, Iwaniec UT, Kim JB, Almeida EA, Damsky CD, Wronski TJ, van der Meulen MC 2004 Skeletal Phenotype of Growing Transgenic Mice that Express a Function-Perturbing Form of beta1 Integrin in Osteoblasts. *Calcif Tissue Int.* (Epub ahead of print).

Grabner B, Landis WJ, Roschger P 2001 Age- and genotype-dependence of bone material properties in the osteogenesis imperfecta murine model (oim). *Bone* **29**:453-457.

Gui Y, Murphy LJ 2001 Insulin-like growth factor (IGF)-binding protein-3 (IGFBP-3) binds to fibronectin (FN): demonstration of IGF-I/IGFBP-3/fn ternary complexes in human plasma. *J Clin Endocrinol Metab.* **86**:2104-10.

Homandberg GA 1999 Potential regulation of cartilage metabolism in osteoarthritis by fibronectin fragments. *Frontiers in Bioscience* **4**:713-730.

Homandberg GA 2001 Cartilage damage by matrix degradation products: fibronectin fragments. *Clin Orthop.* **391**:S100-7

Ingham KC, Brew SA, Migliorini M 2002 Type I collagen contains at least 14 cryptic fibronectin binding sites of similar affinity. *Arch Biochem Biophys.* **407(2)**:217-23.

Jikko A, Harris SE, Chen D, Mendrick D, and Damsky, CH 1999 Collagen integrin receptors regulate early osteoblast differentiation induced by BMP-2. *J Bone Miner Res.* **14**: 1075-1083.

Jones SJ, Glorieux FH, Travers R, Boyde A 1999 The microscopic structure of bone in normal children and patients with osteogenesis imperfecta: A survey using backscattered electron imaging. *Calcif Tissue Int* **64**:8-17.

LaCelle P, Blumenstock FA, Saba T 1991 Blood-borne fragments of fibronectin after thermal injury. *Blood* 77:2037-2041.

Landis WJ 1995 The strength of a calcified tissue depends in part on the molecular structure and organization of its constituent mineral crystals in their organic matrix. *Bone* 16:533-544.

Martin RB, Ishida J 1989 The relative effects of collagen fiber orientation, porosity, density, and mineralization on bone strength. *J Biomech.* 22:419-426.

Martin RB, Boardman DL 1993 The effects of collagen fiber orientation, porosity, density, and mineralization on bovine cortical bone bending properties. *J Biomech.* 26:1047-1054.

Martin B 1993 Aging and strength of bone as a structural material. *Calcif Tissue Int.* 53 (Suppl. 1):S34-S39.

Martin RB, Lau ST, Mathews PV, Gibson VA, Stover SM 1996 Collagen fiber organization is related to mechanical properties and remodeling in equine bone: A comparison of two methods. *J Biomech.* 29:1515-1521.

Masse PG, Rimnac CM, Yamauchi M, Coburn SP, Rucker RB, Howell DS, Boskey AL
1996 Pyridoxine deficiency affects biomechanical properties of chick tibial bone. *Bone*
18:567-574.

McBride DJ Jr, Shapiro JR, Dunn MG 1998 Bone geometry and strength measurements
in aging mice with the oim mutation. *Calcif Tissue Int.* **62**:172-6.

McDonald JA 1988 Extracellular matrix assembly. *Annu. Rev. Cell Biol.* **4**:183-207.

Mehta SS, Oz OK, Antich PP 1998 Bone elasticity and ultrasound velocity are affected
by subtle changes in the organic matrix. *J Bone Miner Res.* **13**:114-121.

Moursi AM, Damsky CH, Lull J, Zimmerman D, Doty SB, Aota S, Globus RK 1996
Fibronectin regulates calvarial osteoblast differentiation. *J Cell Sci.* **109**:1369-80.

Moursi AM, Globus RK, Damsky CH 1997 Interactions between integrin receptors and
fibronectin are required for calvarial osteoblast differentiation in vitro. *J Cell Sci.*
110:2187-96.

van der Meulen MC, Jepsen KJ, and Mikic B 2001 Understanding bone strength: size
isn't everything. *Bone* **29**: 101-104.

Miyamoto S, Teramoto H, Gutkind JS, Yamada KM 1996 Integrins can collaborate with growth factors for phosphorylation of receptor tyrosine kinases and MAP kinase activation: roles of integrin aggregation and occupancy of receptors. *J Cell Biol.* **135**:1633-42.

Nakayamada S, Okada Y, Saito K, Tamura M, Tanaka Y 2003 *J Bio Chem.* **278**:45368-45374.

Pereira RF, Hume EL, Halford KW, Prockop DJ 1995 Bone fragility in transgenic mice expressing a mutated gene for type I procollagen (COL1A1) parallels the age-dependent phenotype of human osteogenesis imperfecta. *J Bone Miner Res.* **10(12)**:1837-43.

Puustjärvi K, Nieminen J, Kasanen T, Hyttinen M, Helminen HJ, Kroger H, Huuskonen J, Alhava E, Kovanen V 1999 Do more highly organized collagen fibrils increase bone mechanical strength in loss of mineral density after one-year running training?. *J Bone Miner Res.* **14**:321-329.

Riggs CM, Vaughan LC, Evans GP, Lanyon LE, Boyde A 1993 Mechanical implications of collagen fibre orientation in cortical bone of the equine radius. *Anat Embryol (Berlin).* **187**:239-248.

Sakata T, Wang YM, Halloran BP, Elalieh HZ, Cao J, Bikle DD 2004 Skeletal unloading induces resistance to insulin-like growth factor-I (IGF-I) by inhibiting activation of the IGF-I signaling pathways. *J Bone Miner Res.* **19**: 436-446.

Sasaki T, Wiedemann H, Matzner M, Chu ML, Timpl R 1996 Expression of fibulin-2 by fibroblasts and deposition with fibronectin into a fibrillar matrix. *J Cell Sci.* **109**:2895-2904.

Sasaki T, Forsberg E, Bloch W, Addicks K, Fassler R, Timpl R 1998 Deficiency of beta 1 integrins in teratoma interferes with basement membrane assembly and laminin-1 expression. *Exp Cell Res.* **238**:70-81.

Schwarzbauer JE 1991 Identification of the fibronectin sequences required for assembly of a fibrillar matrix. *J Cell Biol.* **113**:1463-73.

Sechler JL, Schwarzbauer JE 1998 Control of cell cycle progression by fibronectin matrix architecture. *J Biol Chem.* **273**:25533-6.

Sieg DJ, Hauck CR, Ilic D, Klingbeil CK, Schaefer E, Damsky CH, Schlaepfer DD 2000 FAK integrates growth-factor and integrin signals to promote cell migration. *Nat Cell Biol.* **2**:249-256.

Skrha J, Richter H, Hormann H 1988 Evidence for the presence of a free N-terminal fibronectin 30-kDa domain in human plasma by quantitative determination with an indirect immunosorbent assay. *Anal Biochem* **173**:228-234.

Skrha J, Vackova I, Kvasnicka J, Stibor V, Stolba P, Richter H, Hormann H 1990 Plasma free N-terminal fibronectin 30-kDa domain as a marker of endothelial dysfunction in type I diabetes mellitus. *Eur J Clin Invest* **20**:171-176.

Sottile J, Hocking DC 2002 Fibronectin polymerization regulates the composition and stability of extracellular matrix fibrils and cell-matrix adhesions. *Molecular Biology of the Cell* **10**:3546-59.

Spadaro JA, Werner FW, Brenner RA, Fortino MD, Fay LA, Edwards WT 1994 Cortical and trabecular bone contribute strength to the osteopenic distal radius. *J Orthop Res* **12**:211-218.

Spengler DM, Baylink DJ, Rosenquist JB 1977 Effect of beta-aminopropionitrile on bone mechanical properties. *J Bone Joint Surg.* **59A**:670-672.

Sun BH, Mitnick M, Eielson C, Yao GQ, Paliwal I, Insogna K. 1997 Parathyroid hormone increases circulating levels of fibronectin in vivo: modulating effect of ovariectomy. *Endocrinology* **138**:3918-24

Suzuki K, Ono Y, Umeda M, Itoh H 1992 Secretion of cell-adhesion-promoting factors, fibronectin, fibronectin fragments and a 53-kDa protein, by human rectal adenocarcinoma cells. *Int J Cancer* **52**:818-826.

Tang CH, Yang RS, Liou HC, and Fu WM 2003 Enhancement of fibronectin synthesis and fibrillogenesis by BMP-4 in cultured rat osteoblast. *J Bone Miner Res.* **18**: 502-511.

Thiéry J, Duband J, Dufour S, Savagner P, Imhof, BA 1989 In: Mosher DF (ed.) *Fibronectin*. Academic Press Inc., San Diego, USA, pp. 181-212.

Traub W, Arad T, Vetter U, Weiner S 1994 Ultrastructural studies of bones from patients with osteogenesis imperfecta. *Matrix Biol.* **14**:337-345.

Tuukkanen J, Koivukangas A, Jamsa T, Sundquist K, Mackay CA, Marks SC Jr. 2000 Mineral density and bone strength are dissociated in long bones of rat osteopetrotic mutations. *J Bone Miner Res.* **15**:1905-11.

Velling T, Risteli, J, Wennerberg K, Mosher DF, Johansson S 2002 Polymerization of type I and III collagens is dependent on fibronectin and enhanced by integrins alpha 11beta 1 and alpha 2beta 1. *J. Biol. Chem.* **277**:37377-37381.

Vetter U, Eanes ED, Kopp JB, Termine JD, Robey PG 1991 Changes in apatite crystal size in bones of patients with osteogenesis imperfecta. *Calcif Tissue Int.* **49**:248-250.

Villanueva AR, Kujawa M, Mathews CH, Parfitt AM 1983 Identification of the mineralization front: comparison of a modified toluidine blue stain with tetracycline fluorescence. *Metab Bone Dis Relat Res.* **5**:41-45.

Wojtowicz A, Dzedzic-Goclawska A, Kaminski A, Stachowicz W, Wojtowicz K, Marks SC Jr, Yamauchi M 1997 Alteration of mineral crystallinity and collagen cross-linking of bones in osteopetrotic toothless (tl/tl) rats and their improvement after treatment with colony stimulating factor-1. *Bone* **20**:127-32.

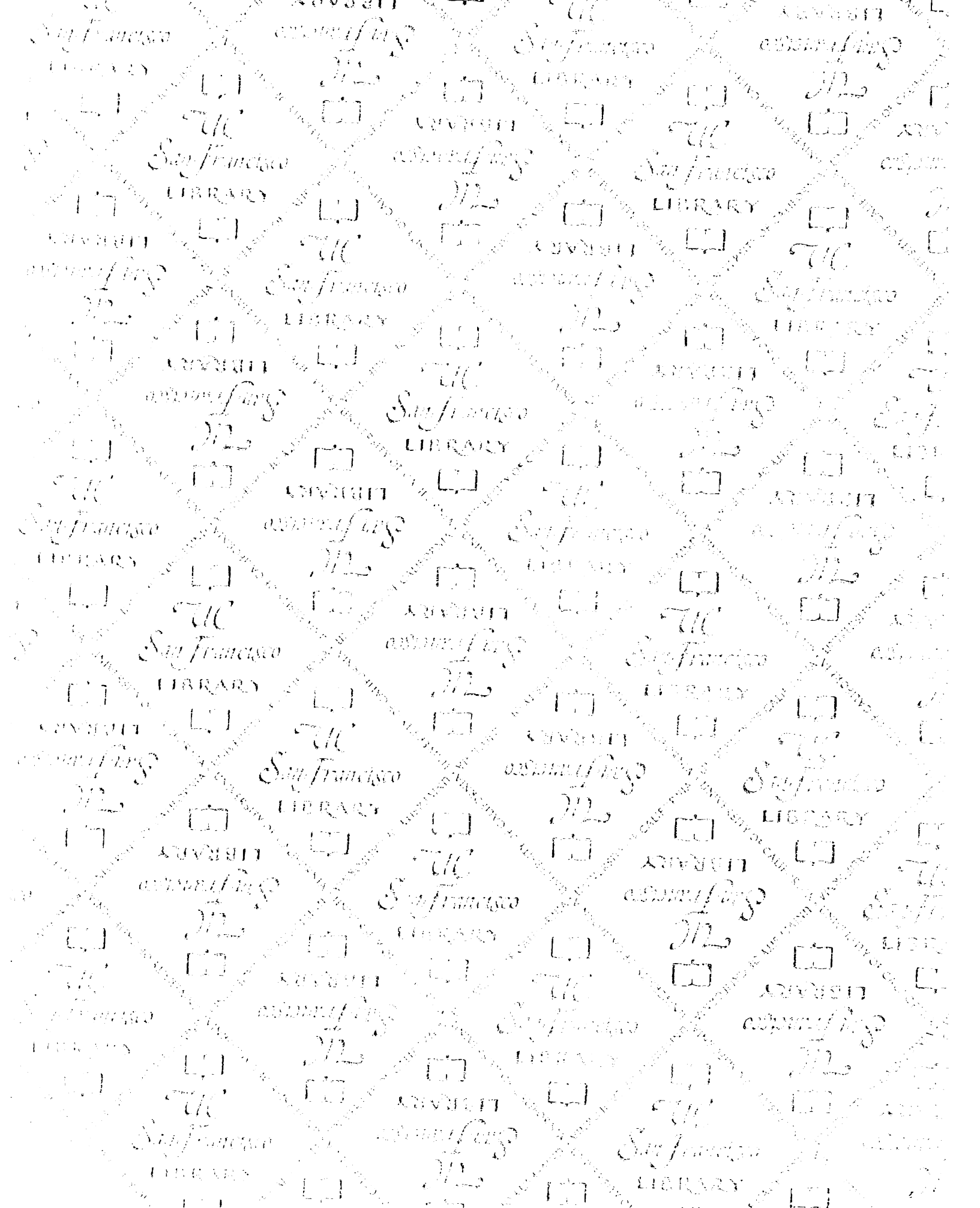
Wolff JJ *Das Gesetz der Transformation der Knochen.* Hirschwald, Berlin, Germany.

Wysocki AB, Grinnell F 1990 Fibronectin profiles in normal and chronic wound fluid. *Lab Invest* **63**:825-831.

Zhao G, Monier-Faugere MC, Langub MC, Geng Z, Nakayama T, Pike JW, Chernausek SD, Rosen CJ, Donahue LR, Malluche HH, Fagin JA, Clemens TL 2000 Targeted overexpression of insulin-like growth factor I to osteoblasts of transgenic mice: increased trabecular bone volume without increased osteoblast proliferation. *Endocrinology*. **141**:2674-82.

Zimmerman D, Jin F, Leboy P, Hardy S, Damsky C 2000 Impaired bone formation in transgenic mice resulting from altered integrin function in osteoblasts. *Developmental Biology* **220**:2-15.

Zoppi N, Gadella R, Paepe AD, Barlati S, Colombi M 2004 Human fibroblasts with mutations in COL5A1 and COL3A1 genes do not organize collagens and fibronectin in the extracellular matrix, down-regulate alpha2beta1 integrin, and recruit alphavbeta3 Instead of alpha5beta1 integrin. *J. Biol. Chem.* **279**:18157-18168.



For reference

Not to be taken from the room.

8071204



3 1378 00807 1204

